Universiteit
Leiden
The Netherlands

Key innate immune components controlling intracellular infection

Benard, E.L.

Citation

Benard, E. L. (2014, September 25). *Key innate immune components controlling intracellular infection*. Retrieved from https://hdl.handle.net/1887/28940

Version:	Corrected Publisher's Version
License:	Licence agreement concerning inclusion of doctoral thesis in the Institutional Repository of the University of Leiden
Downloaded from:	https://hdl.handle.net/1887/28940

Note: To cite this publication please use the final published version (if applicable).

Cover Page

Universiteit Leiden

The handle http://hdl.handle.net/1887/28940 holds various files of this Leiden University dissertation.

Author: Benard, Erica L.
Title: Key innate immune components controlling intracellular infection
Issue Date: 2014-09-25

Chapter 4

Time-resolved transcriptome profiling of the zebrafish host innate immune response to mycobacterium infection

Erica L. Benard, Julien Rougeot, Peter Racz, Herman P. Spaink, Annemarie H. Meijer

Manuscript in preparation

Abstract

Mycobacterium marinum infection in zebrafish embryos is a well-established infection model of mycobacterial pathogenesis. Zebrafish infected with this bacterium develop granulomas similar to *Mycobacterium tuberculosis* infection in humans and the formation of these pathological hallmarks can be visualised in detail in the transparent early larval life stages. To provide a detailed description of the host innate immune response to *M. marinum* infection, we analysed global gene expression levels at multiple time points during infection of zebrafish larvae and interrelated this with imaging data of the infection process and granuloma formation. Our RNA-Seq analysis revealed three distinct phases in the immune response. The early-phase response, during the first hours after phagocytosis of *M. marinum*, is characterised by rapid induction of several transcription factors and a subsequent transient peak of expression of genes linked to pro-inflammatory responses. This is followed by a mid-phase response around 1 day post infection, when expression levels of most genes return to uninfected control levels. Finally, a characteristic late-phase transcriptomal response is initiated when granuloma-like aggregates start forming. This is characterised by increasing expression levels of the same genes that were induced during early-phase and many other inflammation-associated genes. Throughout all phases, profound changes in genes associated with lipid metabolism occur. Notably, the expression profile of a group of apolipoprotein genes is the exact opposite of that of pro-inflammatory genes, showing down-regulation during the early- and late-phase and up-regulation during the mid-phase. In contrast to these dynamic changes in expression, complement components are up-regulated during the entire time course, also during the mid-phase, when other immune related genes show baseline levels. One of the transcription factor genes up-regulated during the early and late phases of infection is *activating transcription factor 3* (*atf3*), which in mice is known to function as a transcriptional repressor of genes involved in the immune response [1, 2]. Embryos in which *atf3* function is inhibited by morpholino treatment have an increased recruitment of macrophages and neutrophils to local inflammatory regions and are better able to control *M. marinum* infection. These results indicate that the induction of *atf3* during *M. marinum* infection antagonises an effective innate immune control of this pathogen.

Introduction

Mycobacterium tuberculosis is a highly successful human pathogen, estimated to have currently infected about one third of the human world population. Host cells express several innate immune pattern recognition receptors (PRRs), such as Toll-like receptors, NOD-like receptors, mannose receptors, scavenger receptors, and complement receptors, that function in the recognition of pathogen associated molecular patterns (PAMPs) of *M. tuberculosis* (reviewed in [3]).This recognition function of the innate immune system provides the first protective barrier of the host against *M. tuberculosis*

and collaborates with the adaptive immune response to control *M. tuberculosis* infection at later stages during infection. The immune response to *M. tuberculosis* infection is not only regulated by the host itself, but also manipulated by the mycobacteria to provide a suitable environment for proliferation, and also promote the immune-mediated responses required for the transmission of disease (reviewed in [4]).

Mycobacterium marinum, a close relative to *M. tuberculosis*, is a natural pathogen of fish and other cold-blooded animals. The genomes of both strains show that there is an *M. marinum* orthologue for 80% of all coding DNA sequences in *M. tuberculosis,* the averaged shared amino acid identity is 85% [5], and many virulence factors found in *M. tuberculosis* have homologous genes in *M. marinum* [6, 7]. Both *M. marinum* and *M. tuberculosis* are capable of surviving and replicating within macrophages. They avoid the bactericidal mechanisms of the macrophage by blocking phagosome-lysosome fusion and both species are also capable of escaping from the phagosome into the cytosol [8-12]. Furthermore, the hallmark of infection with both pathogens is the formation of granulomas, which are highly structured aggregates of infected and non-infected immune cells. Historically these granulomas were strictly regarded as host defence structures containing the infection, but recent insights implicate granulomas, especially the early stages, also in the expansion and dissemination of mycobacterial infection [13].

M. marinum infection of zebrafish shows remarkable resemblance to the human infection with *M. tuberculosis* because caseating granulomas form and latency develops [14, 15]. The transparent embryos and larvae of the zebrafish have become widely used for studying the initial stages of granuloma formation [16, 17]. These studies are facilitated by increasing numbers of fluorescent transgenic zebrafish lines that allow detailed visualisation of the host response towards *M. marinum* infection. *M. marinum* is recognised and phagocytosed extremely rapidly by primitive macrophages following injection into the blood circulation of the zebrafish embryo (Benard et al., chapter 5) [16]. Phagocytosis by macrophages has proven to be an important mechanism of innate immunity, as zebrafish embryos lacking functional leukocytes are not capable of restricting mycobacterial growth [18]. Despite the controlling mechanism of macrophages on the growth of *M. marinum*, this pathogen is still capable of growing restrictedly within these cells. Furthermore, *M. marinum* can direct macrophages to aggregate into granulomas by producing the virulence determinant RD1 (region of deletion 1)-dependent signal [19]. Subsequently, infected macrophages can be seen to leave primary granulomas, either via tissue migration or via the vasculature, and can then initiate secondary granulomas [20]. These events take place during the first few days of zebrafish embryo and early larval development, at which stages an active adaptive immune system is lacking [21]. Thus, the context of innate immunity appears to be sufficient for granuloma formation [16]. Knockdown of tumour necrosis factor receptor 1 (TR1) or knockout of myeloid differentiation factor 88 (*myd88*) have demonstrated the importance of innate immune control in the zebrafish embryo *M. marinum* infection model. In the absence of TNF signalling, *M. marinum* intracellular growth and granuloma formation were

accelerated and followed by necrotic death of overladen macrophages and breakdown of granulomas [22]. Similarly, knockout of *myd88* accelerated formation of granuloma-like aggregates and increased the bacterial burden, which was associated with lower induction of genes central to innate immunity [23].

To support the increasing use of the zebrafish embryo model for *M. marinum* infection, we aimed to provide a detailed time-resolved expression analysis of the innate immune response using RNA deep sequencing (RNA-Seq) technology. We therefore determined RNA-Seq profiles of *M. marinum* infected and non-infected embryos throughout a time course of infection every 2 hours from 2 to 8 hours post infection (hpi) and daily from 1 to 5 days post infection (dpi). To relate these expression profiles to different stages in the infection process, we visualised the host-pathogen interactions over the same time course using a fluorescent macrophage-specific transgenic line in combination with transgenic lines marking neutrophils and endothelial cells of the vascular and lymphatic system. In order to test whether our expression data has functional implications, we analysed the effect of morpholino knockdown of *activating transcription factor 3* (*atf3*) as it is one of a group of transcriptional regulators that showed a significant up-regulation at both early and late stages of infection. We provide evidence that knockdown of *atf3* leads to a decreased mycobacterial load as well as increased macrophage and neutrophil inflammatory migration.

Materials and methods

Zebrafish lines and handling of embryos

Zebrafish were handled in compliance with the local animal welfare regulations and were maintained according to standard protocols (zfin.org). The culture was approved by the local animal welfare committee (DEC) of the University of Leiden and all protocols adhered to the international guidelines specified by the EU Animal Protection Directive 2010/63/EU. Zebrafish lines used in this study included AB/TL, *Tg(fli1a:EGFP)* [24], *Tg(mpx:GFP)*^{i114} [25], *Tg(mpeg1:EGFP)*, and *Tg(mpeg1:mCherry-F)*^{UMSF001} [26]. Embryos were grown at 28.5-30°C in egg water (60 µg/ml Instant Ocean sea salts). For the duration of bacterial injections and imaging, embryos were kept under anaesthesia in egg water containing 200 µg/ml tricaine (Sigma-Aldrich). Embryos used for stereo fluorescence imaging were kept in egg water containing 0.003% 1-phenyl-2-thiourea (Sigma-Aldrich) to prevent melanisation.

Morpholino knockdown

Morpholino oligonucleotides (Gene Tools) were diluted to the desired concentration in 1x Danieau buffer (58 mM NaCl, 0.7 mM KCl, 0.4 mM $MgSO_4$, 0.6 mM $Ca(NO_3)_2$, 5.0 mM HEPES; pH 7.6) containing 1% phenol red (Sigma-Aldrich) and 1 nL was injected into the yolk at the 1-2 cell stage using a Femtojet injector (Eppendorf).

For knockdown of *atf3*, two splice blocking morpholinos were used, morpholino 1 targeting intron 2 – exon 3 and morpholino 2 targeting intron 3 – exon 4 boundaries (*atf3* mo1: 5'GGACAGCCTGAAATAACAACATCTA3', 0.2 mM and *atf3* mo2: 5'CTTCTCAGACTCCTAAAGTCAAAAC3', 0.2 mM) and one translation blocking morpholino (*atf3* ATG: 5'GTGCTGAAGCATCATGCCGAAATCT3', 0.1 mM). As a control the standard control morpholino from Gene Tools was used at the same concentrations as the other morpholinos.

Chemically induced inflammation

Copper sulphate ($CuSO_4$, 10 uM, 2 hours treatment) Merck, #1027910250) was administered via the egg water to induce cell death of neuromast hair cells [27].

Infection experiments

Mycobacterium marinum infections were performed using the wild type Mma20 strain expressing mCherry in a pSMT3 vector (250 cfu) [28] for RNA-Seq, qPCR analysis and imaging experiments. Additionally, when triple-fluorescence imaging was performed, the wildtype M strain expressing E2-Crimson in a pSMT3 vector (250 cfu) [15] was used. Both wild type strains are human isolates and AFLP-DNA fingerprint identifies them both as Cluster I strains which cause acute disease [28]. We observe a similar behaviour in embryonic infection with both wild type strains. Embryos were staged at 24 hpf by morphological criteria [29] and manually dechorionated. Bacteria were prepared and injected into the blood circulation at 28 hpf, and 2% PVP was injected as a control [30].

RNA isolation, cDNA synthesis, and expression analyses

Pools of 30 embryos for RNA isolation were snap frozen in liquid nitrogen and subsequently stored at -80°C. Time course RNA-Seq reactions were performed with four biological replicates. Embryos were homogenized in 0.7 ml of QIAzol® Reagent (Qiagen) and subsequently total RNA was extracted and on-column DNase digestion was performed with a miRNeasy Mini Kit (Qiagen) according to the manufacturer's instructions. RNA sequencing was performed as previously described with a minimum of 10 million reads per sample [31]. qPCR analysis was performed as described [32]. Primers for *il1b* and *mmp9* are described in [33], *apoa4* are described in [34], and *il8* are described in [32]. All data (mean ± SEM) were analysed using unpaired, two-tailed t-tests for comparisons between two groups (*, $p<0.05$; **, $p<0.01$; ***, $p<0.001$). For RNA deep sequencing, significant differences were calculated by DESeq analysis of transcript count data (*=fold change>2, $p<0.05$).

Proportional Venn diagrams were created with a Venn Diagram Generator (http://jura.wi.mit.edu/bioc/tools/venn.php). Gene ontology analysis was performed using DAVID v6.7 (http://david.abcc.ncifcrf.gov/home.jsp) [35]. Gene ontology terms are considered significant when the false-discovery rate was below 5%.

Knockdown of *atf3* with splice morpholino 1 and morpholino 2 was verified by RT-PCR with the SuperScript® One-Step RT-PCR System (Invitrogen, #10928-034) using 50 ng of DNAse treated RNA template. RT-PCR primers for *atf3* Mo1 knockdown verification were FW: 5'ATGTCCAACGGCATGAGCAC3'; REV: 5'GCGGTGTGTGTTGGTCCATT3'. The following adjustments were made to the PCR settings: 59.4°C for 30 seconds for the annealing step with 40 cycles of the PCR amplification. RT-PCR primers for *atf3* Mo2 knockdown verification were FW 5'ATTGTTGATGGGTGGGTGTTG3' RV: 5'TCCTCGATCTGAGCTTTCAGC3'. The following adjustments were made to the PCR settings: 54°C for 30 seconds for the annealing step with 1 min elongation at 72°C with 40 cycles. Morpholino 2 targets the intron3-exon4 boundary site leading to an intron inclusion (exon 4 is the last exon). The RT-PCR primers used were designed to amplify the retained third intron during *atf3* morpholino 2 knockdown. RNA from pools of 30 infected and uninfected *atf3* morphants and control embryos at 4 dpi (one biological replicate) was isolated as described above and RNA sequencing was performed as previously described [31].

Immunohistochemistry

Identification of neutrophils and macrophages was done by immuno-labelling with a leukocyte specific L-plastin antibody and Alexa568/488-conjugated secondary antibody, combined with neutrophil specific staining for myeloperoxidase activity [36].

Image analysis

Fluorescence images were taken with a Leica MZ16FA stereo fluorescence microscope equipped with a DFC420C digital colour camera. Overlay images of bright field and fluorescence stereomicroscopy and merged channel maximum intensity z-stack projections were made and stitched together in Fiji. In *M. marinum* infection experiments, bacterial pixel counts of stereo fluorescence images were analysed using dedicated pixel quantification software (Benard et al., chapter 6) and bacterial pixel counts of stitched confocal images of the tail regions of embryos were analysed with Fiji. E2-Crimson channels (8-bit) were made binary and the 'analyze particle' function was used to determine number of clusters and pixel values per image. All bacterial pixel count data (mean ± SEM) were analysed using unpaired, two-tailed t-tests for comparisons between two groups (***, $p<0.001$). Confocal images were taken on a Leica TCS SPE with a HC APO 20x 0.7 NA objective and a HCX APO 40x 0.8 NA objective or on a Zeiss LSM5 Exciter / AxioObserver with an HC APO 20x 0.7 NA objective.

Results

Timing of events during the *M. marinum* infection process in zebrafish embryos

In this study we used fluorescence markers to visualise the sequence of events during the first days of the mycobacterial pathogenesis in zebrafish embryos up to the early larval stage and interrelated this with a time-resolved RNA sequencing analysis of the host innate immune response. At 40 minutes post infection (mpi) after intravenous injection of a single cell suspension of *M. marinum* (250 colony forming units (cfu)) we observed that the bacteria are completely internalised by predominantly macrophages (*mpeg1:mCherry-F*) (fig. 1A) and at 2 hpi occasionally by neutrophils (*mpx:GFP*) around the site of injection (fig. 1B). Using a combination of transgenic markers for macrophages (*mpeg1:mCherry-F*) and endothelial cells (*fli1a:EGFP*) and E2-Crimson-expressing *M. marinum* we determined that between 6 hours post injection (hpi) and 1 day post injection (dpi) infected cells travel through the vascular system (fig. 1C-G, supplementary movie S1) and can occasionally be observed outside the blood circulation, adjacent to the duct of Cuvier (fig. 1E) and posterior to the transition of the caudal vein and artery (fig. 1G). However, the majority of the infected cells remain within the vasculature during these stages. At 2 dpi *M. marinum* infected macrophages can be observed within the caudal fin of the embryo (fig 1H). In addition, infected cells travel through the intersegmental vessels, the infection spreads from the caudal vein to the dorsal longitudinal lymphatic vessel, and *M. marinum* can also be seen outside the caudal vein (fig. 1I). Between 2 and 5 dpi clusters of *M. marinum* tend to stay in the same position, where they continue to grow and form tight infection structures. During this growth process the structures extend from inside the blood circulation to outside the vessels (fig. 1I-J).

The formation of granuloma-like structures becomes evident by comparing uninfected embryos (fig. 1K-O) with *M. marinum* infected embryos (fig. 1P-Y) obtained from double transgenic zebrafish carrying the macrophage marker *mpeg1:mCherry-F* and the neutrophil marker *mpx:GFP*. At 1 dpi the infected macrophages and uninfected neutrophils are still spread evenly and no clusters of cells can be seen (fig. 1P), quite similar to the macrophage and neutrophil distribution of uninfected embryos (fig. 1K). At 2 dpi the first clusters can be observed consisting of more infected and uninfected macrophages and a few uninfected neutrophils (fig. 1Q). At 3 dpi neutrophils are attracted to the forming tight aggregates of infected macrophages (fig. 1R) and infected neutrophils can be observed for the first time within the granuloma-like structures (supplementary fig. 1A). At 4 dpi the morphology of the infected macrophages changes to a more rounded shape (fig. 1S) and these cells contain a high level of bacterial fluorescence (fig. 1X), indicating that they are severely infected and this phenomenon is even more apparent at 5 dpi (fig. 1T) when the macrophage fluorescence markedly diminishes. At this stage the number of neutrophils surrounding the granuloma-like structure is increased again compared to the previous day and the granuloma structures start protruding the epithelial layer of the embryo (supplementary fig. 1B).

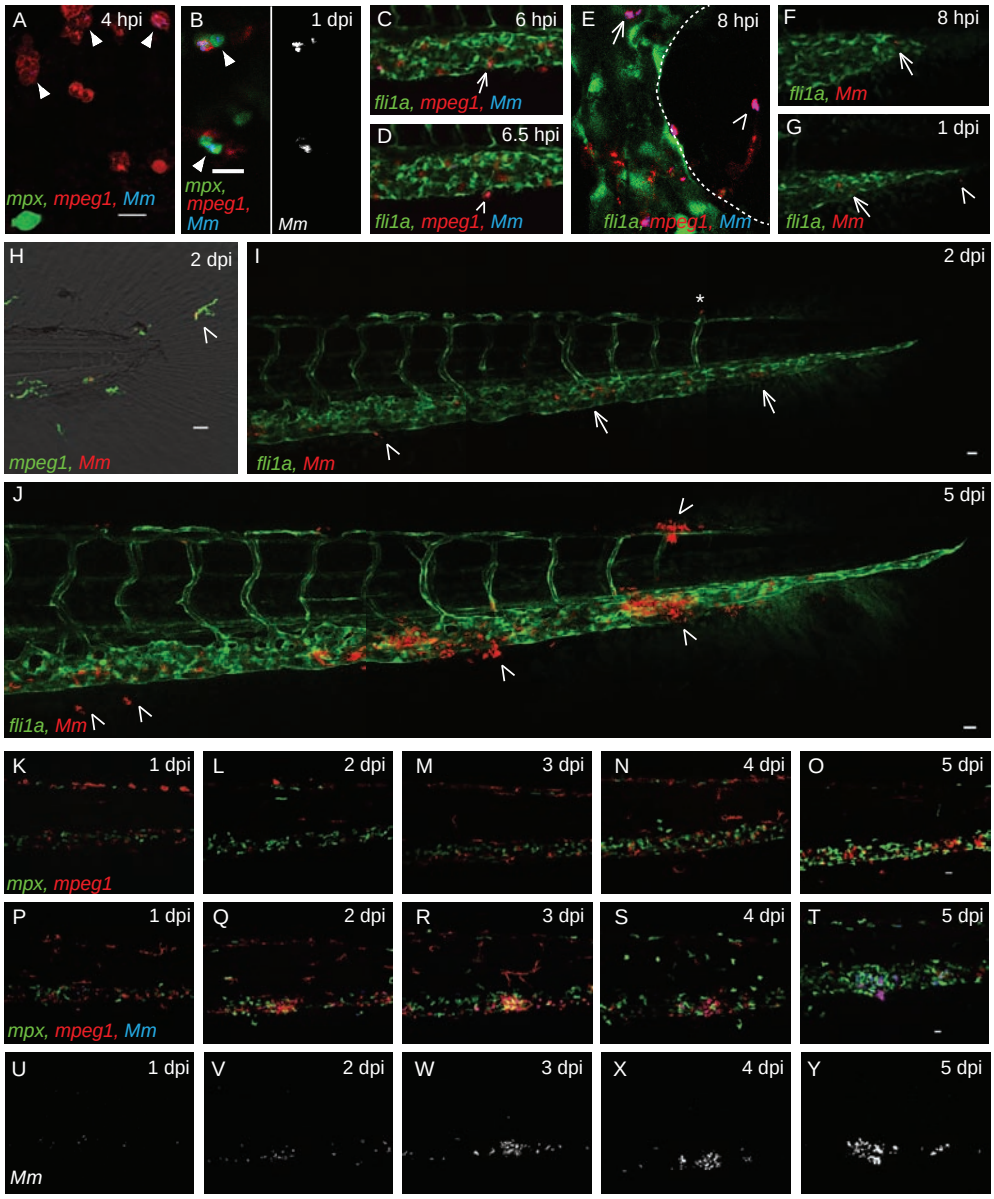

Figure 1. Overview of the *M. marinum* infection process imaged in zebrafish embryos. (A) E2-Crimson-expressing *M. marinum* bacterial infection in *Tg(mpeg1:mCherry-F)/Tg(mpx:GFP)* embryos at 4 hpi imaged at Duct of Cuvier site. Solid arrow heads indicate infected macrophages. (B) E2-Crimson-expressing *M. marinum* bacterial infection in *Tg(mpeg1:mCherry-F)/Tg(mpx:GFP)* embryos at caudal vein site. Left panel: overlay of all three fluorescence channels, right panel: E2-Crimson fluorescence channel with *M. marinum* fluorescence depicted as white pixels. Solid arrowheads indicate infected neutrophils. (C-E) E2-Crimson-expressing *M. marinum* bacterial infection in *Tg(fli1a:EGFP) / Tg(mpeg1:mCherry-F)* embryo imaged over time at (C–D and supplementary movie 1)) the caudal vein at 6 and 6.5 hpi and (E) the Duct of Cuvier site at 8 hpi. *M. marinum* infected macrophages (purple colour: double positive for mCherry and

Figure 1 continued: E2-Crimson) are observed both (arrows) inside and (pointed arrowheads) outside the vasculature. Dotted line in (E) indicates border of vasculature in Duct of Cuvier. (F-G) mCherry-expressing *M. marinum* bacterial infection in a *Tg(fli1a:EGFP)* embryo at the transition of the caudal vein and artery at (F) 8 hpi and (G) 1 dpi. *M. marinum* can be observed (arrow) inside and (pointed arrowhead) outside the vasculature. (H) mCherry-expressing *M. marinum* bacterial infection in a *Tg(mpeg1:EGFP)* embryo imaged at the posterior tail area. Merged image of bright field, GFP and mCherry channels show an infected macrophage (pointed arrowhead) located in the caudal fin. (I-J) mCherry-expressing *M. marinum* bacterial infection in a *Tg(fli1a:EGFP)* embryo imaged at the tail region at (I) 2 dpi and (J) 5 dpi. An *M. marinum* cluster can be seen (asterisk) in the dorsal longitudinal lymphatic vessel and various *M. marinum* clusters can be seen residing (arrow) within the caudal vein and (pointed arrowhead) outside the caudal vein at (I) 2 dpi. These clusters increase in size at (J) 5 dpi and clusters previously inside the caudal vein at 2 dpi are now observed (pointed arrowhead) outside the caudal vein. (K-O) Uninfected (mock injected) *Tg(mpx:GFP)/Tg(mpeg1:mCherry-F)* embryo tail region posterior to the urogenital opening imaged over a time course of (K) 1 dpi, (L) 2 dpi, (MI) 3 dpi, (N) 4 dpi and (O) 5 dpi. Images are z-stack projections of the merged channels of GFP and mCherry. (P-Y) E2-Crimson-labelled *M. marinum* bacterial infection in a *Tg(mpx:GFP)/Tg(mpeg1:mCherry-F)* embryo imaged in identical area as (K-O) uninfected embryo over time course of (P) 1 dpi, (Q) 2 dpi, (R) 3 dpi, (S) 4 dpi and (T) 5 dpi. Images are z-stack projections of the merged channels of GFP, mCherry and E2-Crimson. (U-Y) Z-stack projections of the E2-Crimson channel isolated from P-T and depicted as white pixels. Scale bars: 20 µm.

The profiles of the gene expression response to *M. marinum* infection can be divided into an early, mid, and late-phase

For a detailed characterisation of the host innate immune response during the course of *M. marinum* infection, we sampled pools of 30 embryos every 2 hours from 2 hpi to 8 hpi and daily from 1 dpi to 5 dpi. Four biological replicates of each time point were used for RNA sequencing and DeSeq was used for statistical comparison with mock-injected control embryos sampled at the same time points [37]. At 2 hpi, an immediate response to the infection was observed with 170 up-regulated genes and 64 down-regulated genes. Subsequently, over the time period between 4 hpi and 1 dpi, the total number of differently regulated genes was at least 3-fold lower (55 up and 33 down at 4 hpi, with a further decline between 6 hpi and 1 dpi (fig. 2A, table 1). Subsequently, an increase in up- and down-regulated genes was seen at 2 dpi (310 up and 459 down) which then decreased slightly at 3 dpi but continued to increase remarkably at 4 (1165 up and 748 down) and 5 dpi (1394 up and 668 down) when the embryos were highly infected.

Based on the apparent trend in gene regulation, we divide the transcriptional response in three main phases: an immediate early-phase with a clear response at 2 dpi and rapid decline at 4 hpi, a mid-phase response from 4 hpi to 1 dpi when there is low differential gene regulation, and a late-phase response, which starts from 2 dpi but is mainly characterised by a striking increase in differential gene expression at 4 and 5 dpi (fig. 2A). When we look at the overlap between different time points, we find that there is remarkable little overlap between consecutive time points of the series up to 4 dpi (table 1). For example, in the early phase only 13 up-regulated genes were overlapping between 2 hpi and 4 hpi, and there was no overlap of the down-regulated genes (fig. 2B). The only genes that were significantly up-regulated for each time point during 2 hpi until 8 hpi are the matrix metalloproteinase gene *mmp9* and a non-coding RNA (*si:dkey-97i18.5*). Hardly any overlap can be found when comparing two mid-phase stages (6 hpi with 1 dpi), during which a very low number of genes are differentially regulated (fig. 2B). This is quite the opposite when the final two time points of the late-phase time points are compared (4 dpi with 5 dpi), when a high overlap is evident between the up-regulated genes (table 1). Furthermore, there was also higher overlap between the earliest time point (2 hpi) and the latest time points (4 and 5 dpi). This is reflected in the results of gene ontology (GO) analysis using DAVID [35], which shows up-regulated biological process categories that are identified during both the early-phase and late-phase responses: response to bacterium and proteolysis (fig. 2C and supplementary table 1). In contrast, during the mid-phase response the category of lipid transport is exclusively detected at 1 dpi. Hexose metabolic process, oxygen transport, and muscle contraction are exclusively up-regulated at the beginning of the late phase at 2 dpi (fig. 2C). Notable at this time point was also the down-regulation of genes related to the GO-terms homeostatic process and DNA replication initiation. The up- and down-regulated gene groups at 2 dpi show that the transition between the mid-phase and late-phase in the infection process is associated with strong effects on the host metabolism.

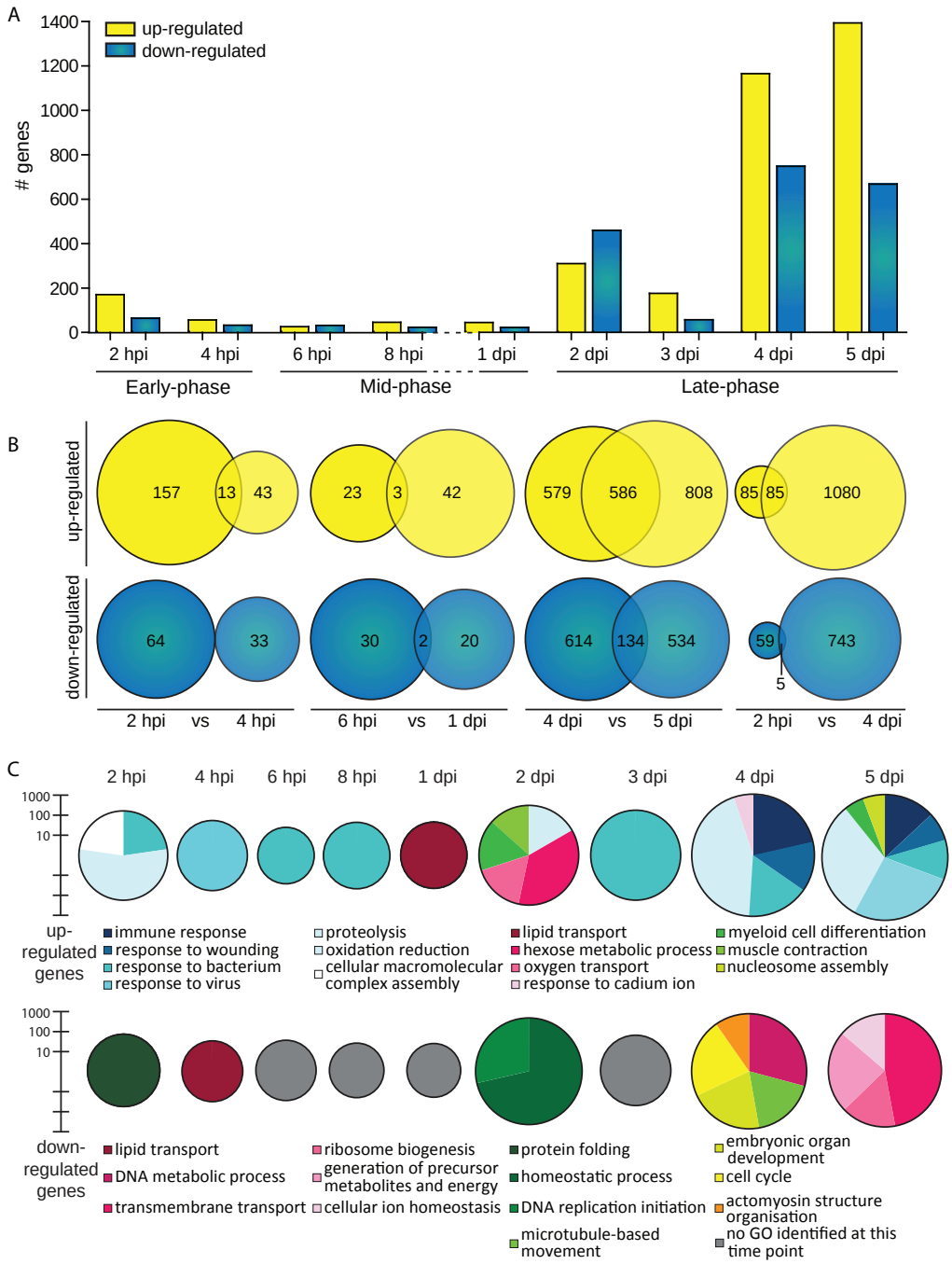

Figure 2. Overview of total number of genes differentially regulated in M. marinum infected embryos, their overlap between various time points and Gene ontology terms enriched per time point. AB/TL embryos were infected with *M. marinum* Mma20 strain at 1 dpf and their expression profiles were compared to their mock-injected control embryos at 2, 4, 6 and

Figure 2 continued: 8 hpi and 1, 2, 3, 4 and 5 dpi. (A) Overview of the total number of genes either significantly up-regulated (yellow) or down-regulated (blue) per time-point in the *M. marinum* infected samples compared to the uninfected control embryos. (B) Area-proportionate Venn-diagrams representing the overlap of both up-regulated and down-regulated genes during *M. marinum* infection. The time points compared are 2 hpi versus 4 hpi, 6 hpi versus 1 dpi, 4 dpi versus 5 dpi, and 2 hpi versus 4 dpi (respectively left versus right circle for each comparison). (C) Gene ontology terms identified per time point represented as pie charts. The diameter of each chart is proportional to the total number of genes up-regulated (top) or down-regulated (bottom) per time point. Colours illustrate the relative proportion of each identified gene ontology term. Genes without associated gene ontology term are not represented in the pie charts (except for time points with no gene ontologies identified).

Table 1: Overlap of genes up- and down-regulated during *M. marinum* time course infection.

# overlap UP	2 hpi	4 hpi	6 hpi	8 hpi	1 dpi	2 dpi	3 dpi	4 dpi	5 dpi
2 hpi	170	13	6	23	18	28	18	85	88
4 hpi		56	7	9	3	29	23	37	38
6 hpi			26	9	3	16	12	17	17
8 hpi				46	21	22	14	20	24
1 dpi					45	20	6	17	14
2 dpi						310	41	70	69
3 dpi							176	83	98
4 dpi								1165	586
5 dpi									1394

# overlap DOWN	2 hpi	4 hpi	6 hpi	8 hpi	1 dpi	2 dpi	3 dpi	4 dpi	5 dpi
2 hpi	64	0	2	3	1	8	4	5	6
4 hpi		33	1	2	2	1	0	6	1
6 hpi			32	2	2	1	0	2	1
8 hpi				23	3	7	0	2	3
1 dpi					22	9	5	3	3
2 dpi						459	6	40	29
3 dpi							57	14	7
4 dpi								748	134
5 dpi									668

There was no overlap between the time points in down-regulated biological process categories (fig 2C). In addition to the strong down-regulation response at 2 dpi, many down-regulated gene groups were detected at 4 and 5 dpi, with gene ontology terms mainly related to DNA and protein metabolism and transmembrane transport.

Detailed analysis of gene expression profiles

Following the global gene ontology analysis, we looked in more detail at the expression patterns of different functional groups of genes over the infection time course. This showed that a major part of the immediate early response to *M. marinum* infection at 2 hpi is the up-regulation of transcription factor genes (fig 3A). These included members of the activating transcription factor (ATF) family, the interferon regulatory factor (IRF) family, the CCAAT/enhancer binding protein family (CEBP), the AP-1 (FOS and JUN family), and the NFκB family. About half of these transcription factor genes were still up-regulated at 4 hpi, after which their expression levels returned to the uninfected control levels between 6 hpi to approximately 3 dpi only to become significantly induced again during the final stage of the late phase response at 4-5 dpi (fig 3A).

Pro-inflammatory cytokines produced by phagocytes, such as tumor necrosis factor alpha (TNF-α) and interleukin 1 beta (IL-1β), play an important role in control of mycobacterial infection. IL-1β expression is tightly controlled by a signal that can induce the expression of pro-IL-1β and a signal that results in the maturation of IL-1β via inflammasome-mediated cleavage by caspase-1 [38]. During *in vivo M. tuberculosis* infection in mice, it was shown that IL-1β is essential for MyD88-dependent host resistance [39]. In zebrafish, the presence of a MyD88-dependent signalling route leading to *il1b* induction has been demonstrated during *M. marinum* infection [23]. The zebrafish genome contains two homologs of the TNF-α gene (named *tnfa* and *tnfb*) [40] and it was demonstrated that a strict balance of TNF-α signalling is essential for control of *M. marinum* infection in zebrafish embryos [41]. During the *M. marinum* infection, up-regulation of *il1b* and both *tnf*-α genes can be observed as well as up-regulation of two chemokine genes, *il8* (*cxcl8*) and *cxcl-c1c*. Similar to its human counterpart, zebrafish *il8* has been shown to mediate neutrophil recruitment [42, 43] and *cxcl-c1c* is an *il8*-related chemokine that is also induced during Salmonella infection [32]. Analysis of the *M. marinum* infection time course shows that there are two apparent waves of significant up-regulation of pro-inflammatory cytokines, the first at 4 hpi when *il1b* , *tnfb* (tumor necrosis factor alpha b), *il8* and *cxcl-c1c* peak and the second at 3 – 5 dpi when *il8* and *cxcl-c1c* are first up-regulated at 3 dpi followed by the additional up-regulation of *il1b* at 4 dpi and *tnfa* (tumor necrosis factor alpha a) and *tnfb* at 4 dpi onwards. Induction of *il1b* and *il8* was confirmed with qPCR analysis (supplementary fig. 2F and G).

Matrix metalloproteinases (MMPs) have been implicated in tissue remodelling and cytokine processing [44]. In zebrafish, *mmp9* has been shown to play an important role during *M. marinum* infection by facilitating the recruitment of leukocytes to the site of infected macrophages (fig. 1P-T) [45]. *mmp9* as well as *mmp13a* were found to be significantly up-regulated at most time points during the course of infection (fig. 3C) and the observed up-regulation of *mmp9* was confirmed with qPCR analysis (supplementary fig. 2H). A similar pattern was observed for the expression of *tissue inhibitor of metalloproteinase 2b* (*timp2b*), presumably functioning to avoid excess tissue damage by inhibiting the strongly induced MMPs. TIMPs can bind in a non-covalent manner to the catalytic domain of MMPs, thus regulating their activity [46]. Other metalloproteinases, such as members of the ADAM (A Disintegrin And Metalloproteinase) family, were only up-regulated during the late-phase of infection (supplementary fig. 2A).

Remarkably, a group of 10 genes related to lipid metabolism and transport appeared to be co-regulated, showing strong fluctuations throughout the infection process. This group of 9 apolipoprotein genes and a fatty acid binding protein gene (*fabp1b.1*) was first up-regulated at 2 hpi and subsequently down-regulated at 4 hpi (fig. 3D), exactly coinciding with the transient peak in pro-inflammatory cytokine induction (fig. 3B)). The down-regulation of *apoa4* at the 4 dpi time point was confirmed with qPCR analysis (supplementary fig. 2I). After the down-regulation at 4 hpi, the gene group was notably up-regulated again between 8 hpi and 2 dpi, and subsequently showed another trend

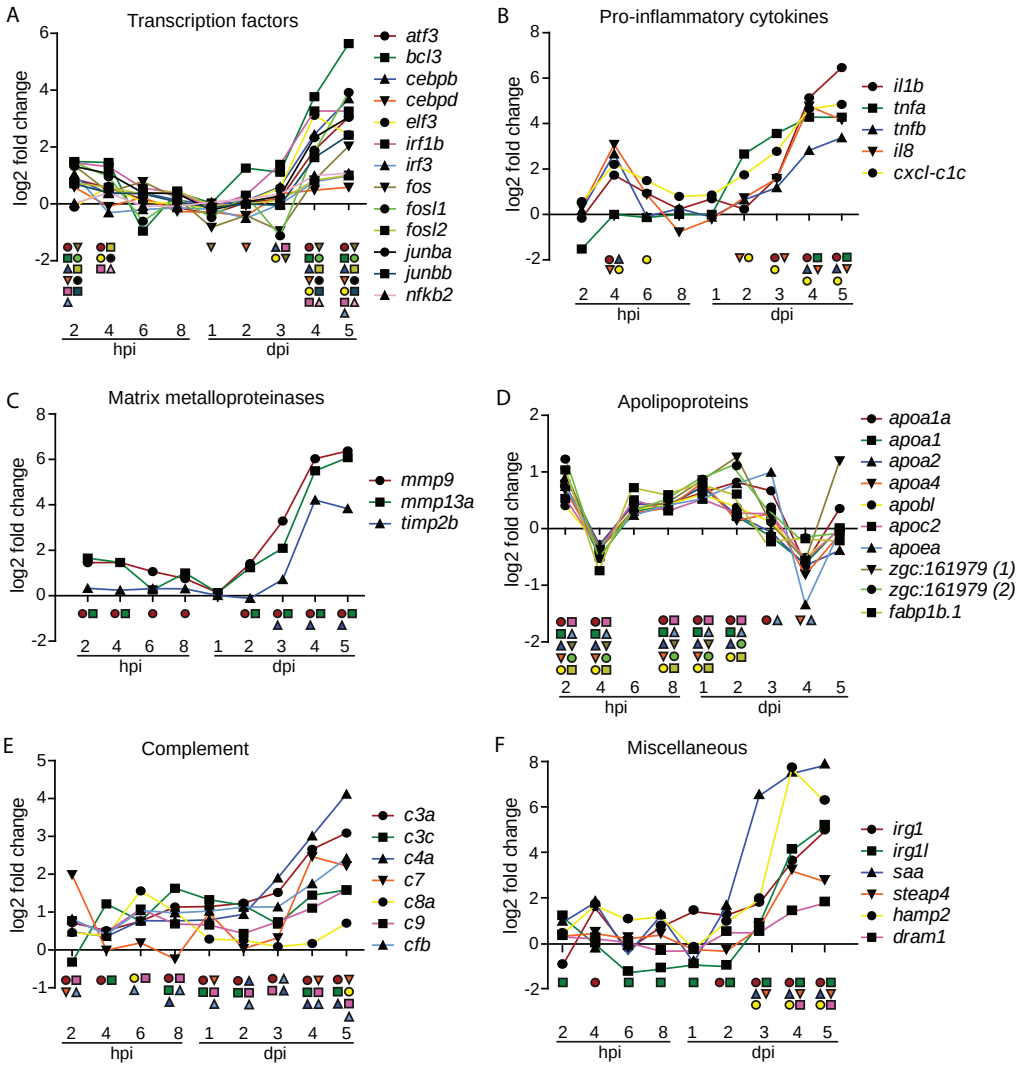

Figure 3. Overview of gene expression profiles during *M. marinum* infection. Gene expression levels of groups of selected genes during a time course of *M. marinum* infection are represented as log2 fold change values. Groups of genes represented are: (A) transcription factors; (B) pro-inflammatory cytokines and chemokine cxcl-c1c; (C) matrix metalloproteinases and inhibitor; (D) apolipoproteins; (E) complement components; (F) miscellaneous late-phase responses. Statistically significant data points (adjusted P-value <0.1) are indicated below the x-axis as the shape filled with the colour of the specific gene (see legend for gene shape and colour). Gene IDs and descriptions can be found in supplementary table 2. Only genes are shown for which differential expression was significant in at least one time point.

towards down-regulation at 4 dpi, but significant only for some genes in the group. The way these genes are regulated is quite remarkable because they are the few genes that are collectively up-regulated during the mid-phase period of the *M. marinum* infection time course, when differential expression of other genes is minimal.

Complement can be immediately activated in response to an invading pathogen and it has been reported that maternal complement components are present in zebrafish eggs [47]. Here, we observed that the expression levels of complement components such as *c3a*, *c7*, *c9,* and *cfb* are rapidly up-regulated by *M. marinum* infection at 2 hpi (fig. 3A). In the subsequent stages of infection different complement components continue to show up-regulated expression. Thus, this is one of the few up-regulated gene groups during the mid-phase, similar to the apolipoprotein gene group. However, in contrast to the apolipoprotein genes, expression of complement genes strongly increased during the late-phase of infection (4-5 dpi) (fig. 3A).

In addition to the above mentioned functional gene groups, we present in Fig. 3F the expression profiles of a miscellaneous group of genes that were previously shown to be important during infection, including: the genes for mitochondria-localising enzymes encoded by *immunoresponsive gene 1-like* (*irg1l*) and *immunoresponsive gene 1* (*irg1*), which was shown to augment bactericidal activity of macrophage-lineage cells by regulating β-oxidation-dependent mitochondrial ROS production [48]; the acute phase response gene *serum amyloid A* (*saa*), an apolipoprotein family member highly expressed in response to inflammation and tissue injury [49]; the metalloreductase gene *six transmembrane epithelial antigen of prostate 4* (*steap4*) (also known as *tumor necrosis factor alpha-induced protein 9* (*tnfaip9*) or *six-transmembrane protein of prostate 2* (*stamp2*), which was shown to play a role in integration of inflammatory and metabolic responses and previously linked with *M. marinum* expression in zebrafish [50-52]; the *hepcidin antimicrobial peptide 2* (*hamp2*) gene involved in microbial killing [53], and the autophagy modulator gene *DNA-damage regulated autophagy modulator 1* (*dram1)*, which our laboratory recently showed to protect against mycobacterial infection in zebrafish [54]. All these genes are strongly up-regulated during the late phase of infection at 4 and 5 dpi, while *irg1* and *irg1l* additionally show up- or down-regulated expression also at earlier time points (fig. 3F). Concomitant with the up-regulation of this miscellaneous group of genes during the late-phase of infection, three other groups of genes are up-regulated, namely a group of prostaglandin genes (supplementary fig. 2C), a group of genes coding for various negative regulators of the immune response (supplementary fig. 2D), and a group of NADH oxidase complex genes (supplementary fig. 2E).

Atf3 impairs control of bacterial growth

Activating transcription factor 3 (*atf3*) is one of the transcription factor genes that we observed to be up-regulated during the early-phase response at 2 and 4 hpi and during the late-phase response at 4 and 5 dpi (fig. 4A). Human ATF3 belongs to the cAMP responsive element-binding (CREB) protein family of transcription factors and is characterised as an immediate early response gene that is induced in cells exposed to a variety of stress stimuli [55]. We chose a morpholino knockdown approach to determine whether *atf3* has an effect on the bacterial growth of *M. marinum*. Knockdown of *atf3* with a splice blocking morpholino resulted in a significantly reduced bacterial burden at 4 dpi compared to the control embryos (fig. 4B and E; supplementary fig. 3A). This effect could be pheno-copied with a second splice blocking morpholino (fig. 4C and F; supplementary fig. 3B) and with a morpholino targeting the translational start site (fig. 4D and G). Since knockdown of *atf3* results in a better control of *M. marinum* infection, we conclude that the transcriptional up-regulation of *atf3* is not a host beneficial response in acute infection in zebrafish larvae.

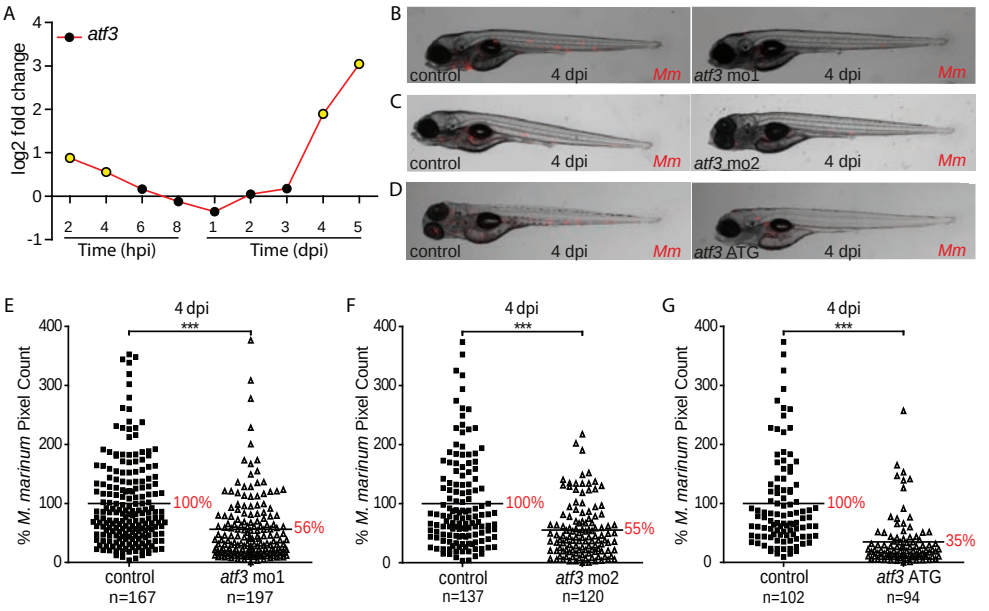

Figure 4. Regulation and function of *atf3* in promoting *M. marinum* infection. (A) Gene expression levels of *atf3* during *M. marinum* time course, represented as log2 fold change in RNA-Seq data compared with uninfected control. Light colouring of a data point indicates that *atf3* expression in infected embryos was significantly different from uninfected controls at this time point. (B-D) Representative overlay images of infected *atf3* (B) splice blocking morpholino 1 (mo1), (C) splice blocking morpholino 2 (mo2), (D) translation blocking morpholino (ATG) injected morphants and their infected standard control morpholino injected controls. (E-G) Bacterial burden of each group was quantified by determining the number of fluorescent bacterial pixels with dedicated software. Graphs show combined percentages of bacterial pixel counts of 3 (E-F) or 2 (G) repeated independent experiments with the standard control mean set to 100%. Each data point represents an individual embryo.

atf3 morphants show minor alterations in the immune response to *M. marinum* infection

To determine whether the morphants of *atf3* have a differently regulated immune response to *M. marinum* we performed RNA sequencing analysis on pools of infected and non-infected *atf3* morphants (splice blocking morpholino 1) and compared this to their control morpholino injected embryos at 4 dpi, a time point when partial knockdown is observed (supplementary fig. 3A) and the morphants have a significantly reduced bacterial burden (fig. 4B and E). We focussed this comparison on the set of genes previously identified during the RNA-Seq analysis of *M. marinum* infection time course (fig. 3). Under infected circumstances, the most notable difference in gene expression levels was in the apolipoprotein and complement gene groups, where all genes showed a lower expression trend in the infected *atf3* morphants compared to the infected control embryos, although only significant for a few of these genes, namely *apoea*, *zgc:161979* (apolipoproteins A-II family*), fabp1b.1*, and *c7.* In addition, in the miscellaneous gene group *hamp2* showed significantly lower expression in infected *atf3* morphants (supplementary fig. 4). The only gene of the set of genes previously selected to show an induction in infected *atf3* morphants compared to infected controls was *irg1l*. None of the genes previously mentioned were significantly up- or down-regulated in uninfected *atf3* morphants compared to uninfected control embryos with the exception of *c3c*, which was down-regulated (fold change 0.48, adjusted p-value 0.026). We also examined expression of pro-inflammatory cytokines and *mmp9* at 4 hpi by qPCR, but found no difference in the transient induction of these genes by infection at this time point or in their basal expression levels in the *atf3* morphants (data not shown). Thus, we conclude that loss of *atf3*, while significantly improving *M. marimum* growth control, had a relatively minor effect on the gene expression response to *M. marinum* infection.

Atf3 suppresses macrophage and neutrophil inflammatory migration

During *M*. *marinum* infection, macrophages and neutrophils are recruited to the site of granuloma formation (fig. 1P-T). Knockdown of *atf3* did not affect total numbers of macrophages and neutrophils (supplementary fig. 3C). We next determined if Atf3 affects the migration of leukocytes and used a chemically induced inflammatory (ChIN) assay [27] to test this on *atf3* morphants and their controls. When the neuromast hair cells of the lateral line were damaged by copper sulphate treatment in this assay, the *atf3* morphants showed increased numbers of both macrophages and neutrophils surrounding the damaged hair cells (fig. 5). This indicates that Atf3 plays an inhibiting role on the migration of leukocytes towards local inflammation sites.

To determine whether the observed increased attraction of macrophages and neutrophils towards inflammatory sites also occurs during *M. marinum* granuloma formation, we imaged *M. marinum* infected individual transgenic embryos with fluorescent macrophages *Tg*(*mpeg1:mCherry-F*) and neutrophils *Tg*(*mpx:GFP*) injected

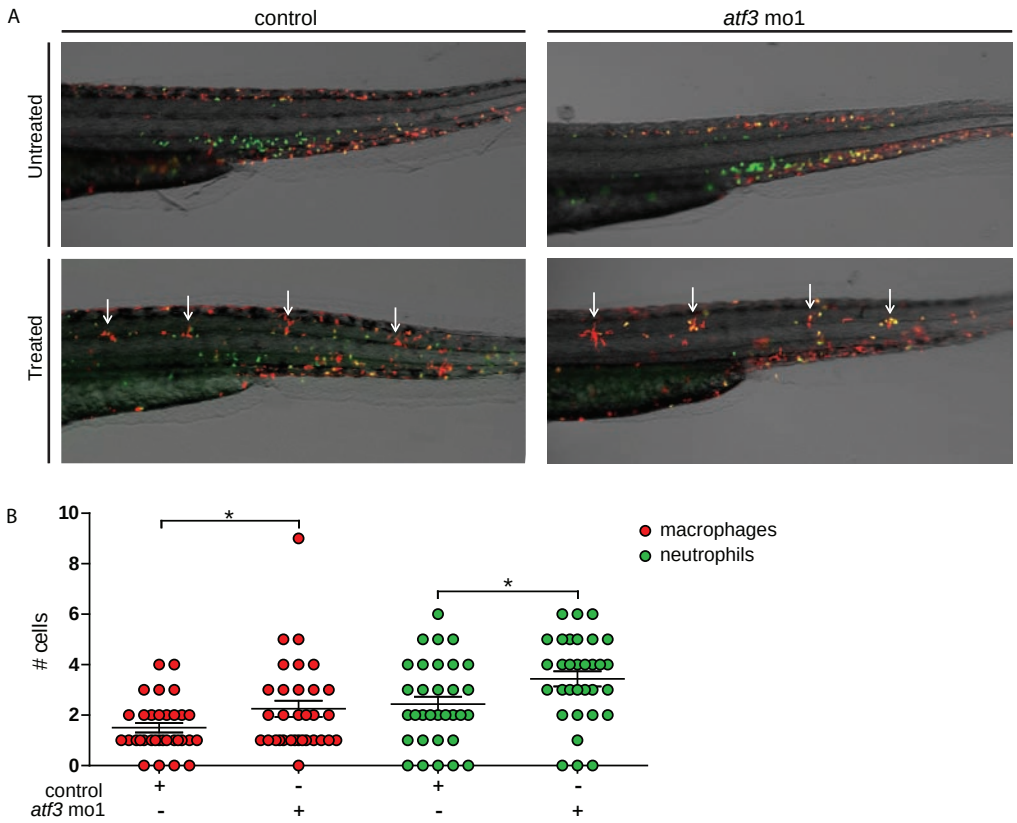

Figure 5. Atf3 inhibits macrophage and neutrophil migration to local inflammation sites. (A) Representative images of untreated and copper sulphate treated control and *atf3* mo1 morphant 3 dpf embryos. Embryos were immuno-labelled with Ab against the general leukocyte marker L-plastin (red signal) in combination with a neutrophil-specific Mpx TSA-staining (green signal). White arrows indicate accumulation of leukocytes at the local inflammation sites of the neuromasts. (B) Number of macrophages and neutrophils surrounding each neuromast site in the copper sulphate treated groups. Each data point represents cells surrounding one neuromast site of individual embryos (3 neuromast locations per embryo) and the mean ± SEM is indicated. Asterisks indicate significant differences (*, $p<0.1$) tested by unpaired t-test.

Figure 6. Detailed visualisation of granuloma formation in atf3 morphants. (A) Region imaged for visualising granuloma formation (red dotted rectangle). (B) Quantified levels of *M. marinum* pixels show that the imaged *atf3* morphant (C) has a decreased total pixel value and decreased number of clusters of *M. marinum* compared to the control embryo (C) in the tail region from 2 dpi onwards, indicating that this morphant is representative for the large pool of *atf3* morphants analysed in figure 4. (C) Merged channel z-stack projections of E2-Crimson-expressing *M. marinum* infection in an *atf3* morphant and a control embryo of the transgenic *Tg(mpeg1:mCherry-F)/Tg(mpx:GFP)* line at 4 hpi (single z-stack), 1 and 2 dpi (two stitched z-stacks), and 3 and 4 dpi (three stitched z-stacks). Macrophages are red, neutrophils are green and *M. marinum* is blue. Scale bars: 20 µm.

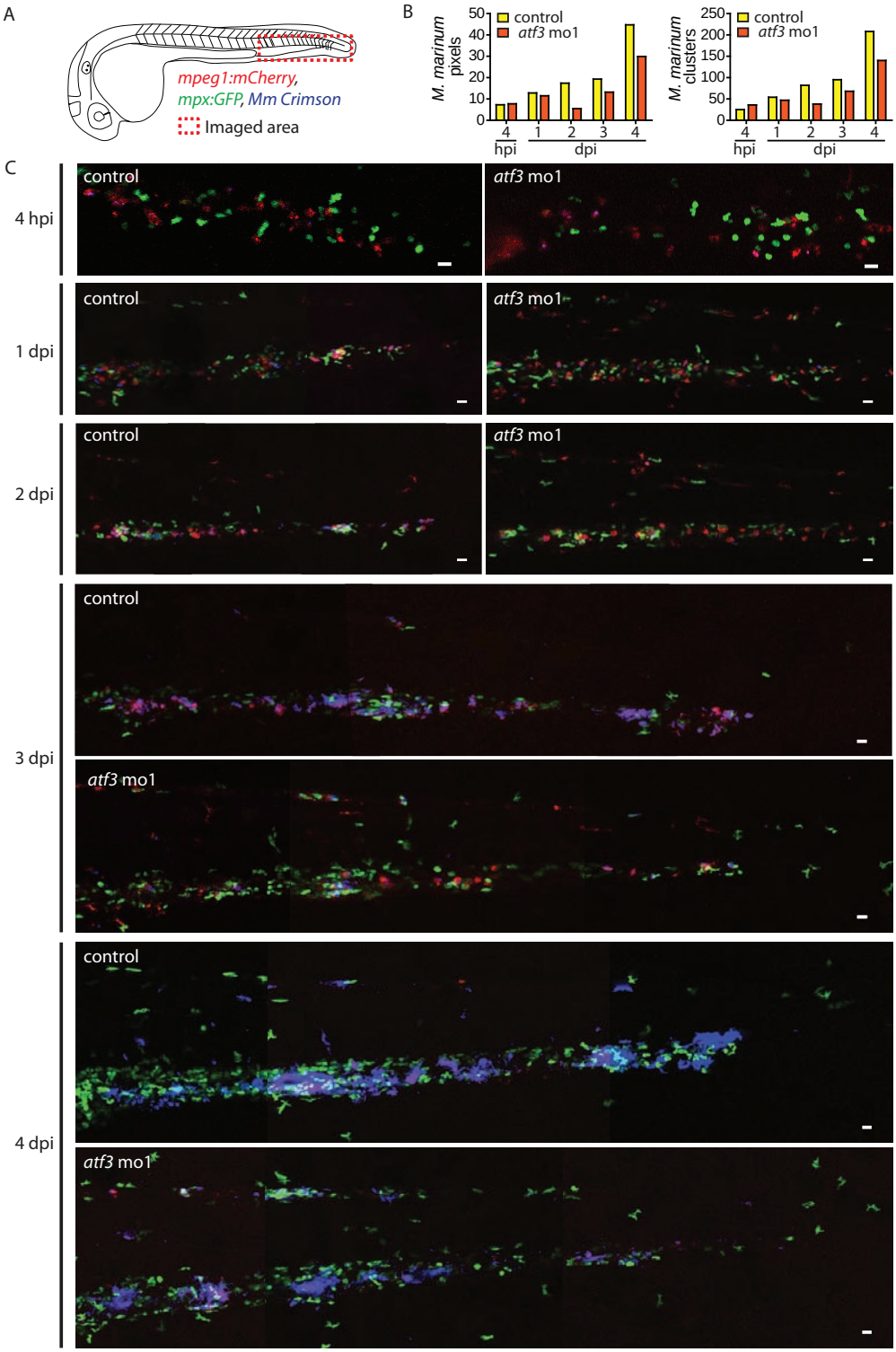
A
mpeg1:mCherry,
mpx:GFP, Mm Crimson
Imaged area
B
M. marinum pixels
control
atf3 mo1
hpi
dpi
M. marinum clusters
C
4 hpi
1 dpi
2 dpi
3 dpi
4 dpi
control
atf3 mo1

with *atf3* morpholino 1 or a control morpholino. The infection process was imaged in the tail region posterior to the urogenital opening (fig. 6A) over a time course starting at 4 hpi and continuing daily from 1 dpi until 4 dpi. Consistent with our previous results (Fig. 4), we observed that despite both embryos starting with an equal dose of infection, the *atf3* morphant had less *M. marinum* pixels and clusters in the tail at 4 dpi compared to the control embryo (fig. 6B). Both embryos showed macrophages containing *M. marinum* and an evenly spread leukocyte pattern at 4 hpi (fig. 6C). This changed at 1 dpi when the distribution of leukocytes appeared to be different in the *atf3* morphant compared to the control embryo: higher numbers of leukocytes were observed in the infected tail region of the *atf3* morphant, although both embryos showed leukocyte accumulation around the *M. marinum* bacteria. A similar difference in leukocyte accumulation was observed at 2 dpi when for the first time a difference in bacterial load was also apparent, reflected by less *M. marinum* fluorescent pixels in the *atf3* morphant (fig. 6B). At 3 dpi spreading of infection to the dorsal side of the tail could be observed in both the control embryo and the *atf3* morphant and at 4 dpi the control embryo had higher *M. marinum* infection. This is also the stage when both embryos no longer had detectible levels of *mpeg1*-promoter driven mCherry fluorescence, however the highly infected control embryo now seemed to have more neutrophils (*mpx*-promoter driven GFP fluorescence) surrounding the granulomas. In conclusion, increased leukocyte attraction at the stage when granuloma formation is first initiated (1-2 dpi) and prior to the inflammatory gene expression response at the later stage of granuloma formation (4-5 dpi), might be the explanation for the better ability of *atf3* morphants to control *M. marinum* infection.

Discussion

Distinct phases in the host response to *M. marinum* infection

The zebrafish *M. marinum* infection model has provided new insights into the development and function of granuloma-like structures, which are the hallmark of infection with pathogenic mycobacteria, including the human pathogen *M. tuberculosis* [17]. Despite the wide use of this model, the innate immune response of zebrafish embryos to *M. marinum* infection, especially during the early stages of infection, had not yet been well characterised. Previous microarray data had shown that early after infection (8 hpi), the host response to *M. marinum* is minimal, in sharp contrast with the strong pro-inflammatory response of zebrafish embryos to other pathogens like *Edwardsiella tarda* and *Salmonella typhimurium*, which cause acute disease [56]. As reported in here, detection of more subtle changes in gene expression during *M. marinum* infection required RNA deep sequencing with four biological replicates. We performed this RNA-Seq analysis over a time course from 2 hpi up to 5 dpi and visualised the host-pathogen interactions throughout the infection process until granuloma formation in order to interrelate the infection stages with the host gene expression profiles. As summarised in figure 7, our gene expression profiles reveal three main phases in the host response: early-phase: induction of complement and transcription factors followed by induction of pro-inflammatory cytokines within hours after phagocytosis of *M. marinum*; mid-phase: minimal response between 6 hpi to 1 dpi when the tissue dissemination of *M. marinum* has begun, except for the induction of complement and apolipoprotein genes; late-phase: progressively increasing induction of complement, transcription factors, pro-inflammatory cytokines, matrix metalloproteinases, and other defence and inflammation related gene groups, along with the expansion of granulomas.

Mycobacterial recognition is an essential step for phagocytosis by macrophages and this process is mediated by pattern recognition receptors (PRRs) [57-59]. In response to recognising *M. marinum*, macrophages rapidly phagocytose the bacteria (fig. 1A) and transcription factors with well-established functions in immunity (for example *atf3*, *jun* and *fos*, and the *irf* family members) are significantly up-regulated at 2 hpi (fig. 3A). Directly after the early peak of transcription factor induction, an induction of pro-inflammatory cytokines and chemokines (*il1b*, *tnfa*, *il8,* and *cxcl-c1c*) occurs at 4 hpi (fig. 3B). During this early-phase response between 2 and 4 hpi, the matrix metalloproteinases *mmp9* and *mmp13a* are also induced (fig. 3C). The timing of this early induction is not surprising because Mmps are known to function in cleaving cytokines and chemokines to augment or to inhibit their functional activity [60, 61]. A second function of Mmps is to degrade components of the extracellular matrix [62], thereby allowing immune cells to migrate to sites of inflammation from the bloodstream. In this infection model, macrophages do not need to migrate towards the infection site because they phagocytose *M. marinum* following injection into the blood circulation; however, after phagocytosis the infected cells migrate outside the vascular system by traversing

endothelial barrier and migrate into tissue (fig. 1C-E and supplementary movie S1) [18] which requires proteolysis of the basement membrane by metalloproteinases. At 2 dpi and 3 dpi, when uninfected macrophages (fig. 1M) and neutrophils (fig. 1N) are first attracted to the forming granulomas (which requires cytokine dependent leukocyte attraction and extracellular matrix degradation), pro-inflammatory cytokines (fig. 3B) and *mmp9* and *mmp13a* (fig. 3C) are once again up-regulated. This induction increases over time until 5 dpi, the time point when the granuloma structures start protruding the epithelial layer (supplementary fig. 1B) and infected macrophages can leave the granuloma to form new granulomas [20]. The increasing expression of *mmp9* during this period is consistent with its proposed function in facilitating the recruitment of macrophages during granuloma formation [45].

A proper balance in immune regulation is essential for the host to suppress bacterial growth. It has been shown that an imbalance in MMP production can also be host-damaging during mycobacterial infection [63-69]. Therefore, it is coherent that the *tissue inhibitor of metalloproteinase 2b* (*timp2b*) is also induced together with *mmp9* and *mmp13a* (fig. 3C). In addition, susceptibility to *M. marinum* in zebrafish can result from either inadequate or excessive acute inflammation [36, 70], therefore it is not surprising that concomitant with the induction of pro-inflammatory genes and transcriptional activators, numerous negative regulators of the TLR pathway (*irak3*, *socs3a*, and a group of NFκB inhibitors) are up-regulated during early- and late-phase infection (supplementary fig. 2D). We have shown that a similar induction of negative regulators occurs during *S. typhimurium* infection [32, 36].

When mycobacteria are intracellular, they can release mycobacterial lipids which are incorporated into exocytosing vesicles of macrophages [71] which allows the mycobacterial lipids to be transferred between cells. This process is mediated by host apolipoprotein E [72], one of the group of apolipoproteins that is also found to be differentially regulated during *M. marinum* infection (fig. 3D). By transferring antigenic lipids from cell to cell, such as TDM, the pathogen can extend its area of influence beyond its own host cell such as attracting cells to form a granuloma-like structure in a myd88-dependent manner in mice [73], similarly to the effect that secreted virulence factor ESAT-6 has on enhancing recruitment of macrophages in a Mmp9-dependent manner in zebrafish [45]. When studying the response of apolipoprotein genes during *M. marinum* infection, we observed a collective regulation of lipoproteins (fig. 3D). Not only are they collectively regulated, they also show a strong fluctuation between up-and down-regulation during the infection process and are the only group of genes, besides complement, that are up-regulated during the mid-phase of infection. This rapid fluctuation in regulation makes the apolipoprotein family intriguing to investigate further. It is not yet known whether these apolipoproteins function similarly in zebrafish and whether *M. marinum* is also capable of modulating cell function via apolipoproteins.

Numerous complement components in zebrafish are transferred from mother to egg as proteins or mRNA [47], thus, protecting the embryo before it is capable of synthesizing

immune-relevant molecules. As mentioned previously, complement is slightly up-regulated during early- and mid-phase infection and is highly induced during late-phase infection when the granuloma matures (fig. 3E). This indicates that already at 1 dpf, the zebrafish embryo itself is capable of inducing complement components in response to *M. marinum* infection. It has been shown that complement component C3 on the surface of *M. tuberculosis* mediates phagocytosis of this bacterium [58] and recently, all the homologs of the mammalian complement fundamental components were found to be present in zebrafish as revealed by phylogenetic analysis [74]. Therefore, it is possible that zebrafish c3a and c3c function in the same manner to assist phagocytosis of *M. marinum*, a process which occurs progressively during granuloma maturation.

During the granuloma maturation, infected cells containing high numbers of *M. marinum* undergo cell death and are phagocytosed by multiple newly recruited macrophages [20]. This process seems beneficial for the mycobacteria because the granuloma expands in this manner. However, dead macrophages also attract neutrophils which are capable of exerting antimicrobial functions against *M. marinum* via inducible Nitric Oxide Synthase (iNOS) signalling [75] and are capable of phagocytosing dying infected macrophages after which they can kill internalised mycobacteria through NADPH-oxidase dependent mechanisms [76]. We observe neutrophils containing *M. marinum* as soon as 1 dpi around the injection site (fig. 1B) and at 3 dpi within the granuloma-like structures (supplementary fig. 1A). In addition, genes of the phagocyte oxidase complex are induced significantly at 4 and 5 dpi (supplementary fig. 2E), which correlates with the infection stage where infected macrophages start dying and increasing numbers of neutrophils are attracted to the maturing granuloma (fig. 1S and T). These results support that neutrophils play an important role during this stage of infection when macrophages are no longer capable of containing mycobacterial growth. Many other defence related genes are induced at this stage of granuloma expansion and the host transcriptome response now has a clear pro-inflammatory signature similar to that observed within hours after infection with the acute pathogens *E. tarda a*nd *S. typhimurium* [56]. In contrast, our time course analysis suggests that during the first days of infection *M. marinum* is capable of suppressing host pro-inflammatory signalling, allowing its replication in macrophages and the initiation of granulomas.

The infection-inducible host transcription factor Atf3 antagonises the control of *M. marinum* growth after acute infection

The RNA sequencing expression profiles allow us to hypothesise which genes play a role during infection with *M. marinum*. We chose to study *atf3* because it is one of the transcription factor genes that is up-regulated during the early- and late-phase host response (fig. 3A). ATF3 is a member of the CREB/ATF family of basic leucine zipper transcription factors. It has been shown to act primarily as a repressor, but splice forms that are unable to bind DNA can also stimulate transcription presumably by sequestration of inhibitory co-factors [77]. In mice, ATF3 is used as an ER stress marker that is expressed in the macrophage-rich area of *M. tuberculosis*-induced granulomas [78]. When analysing

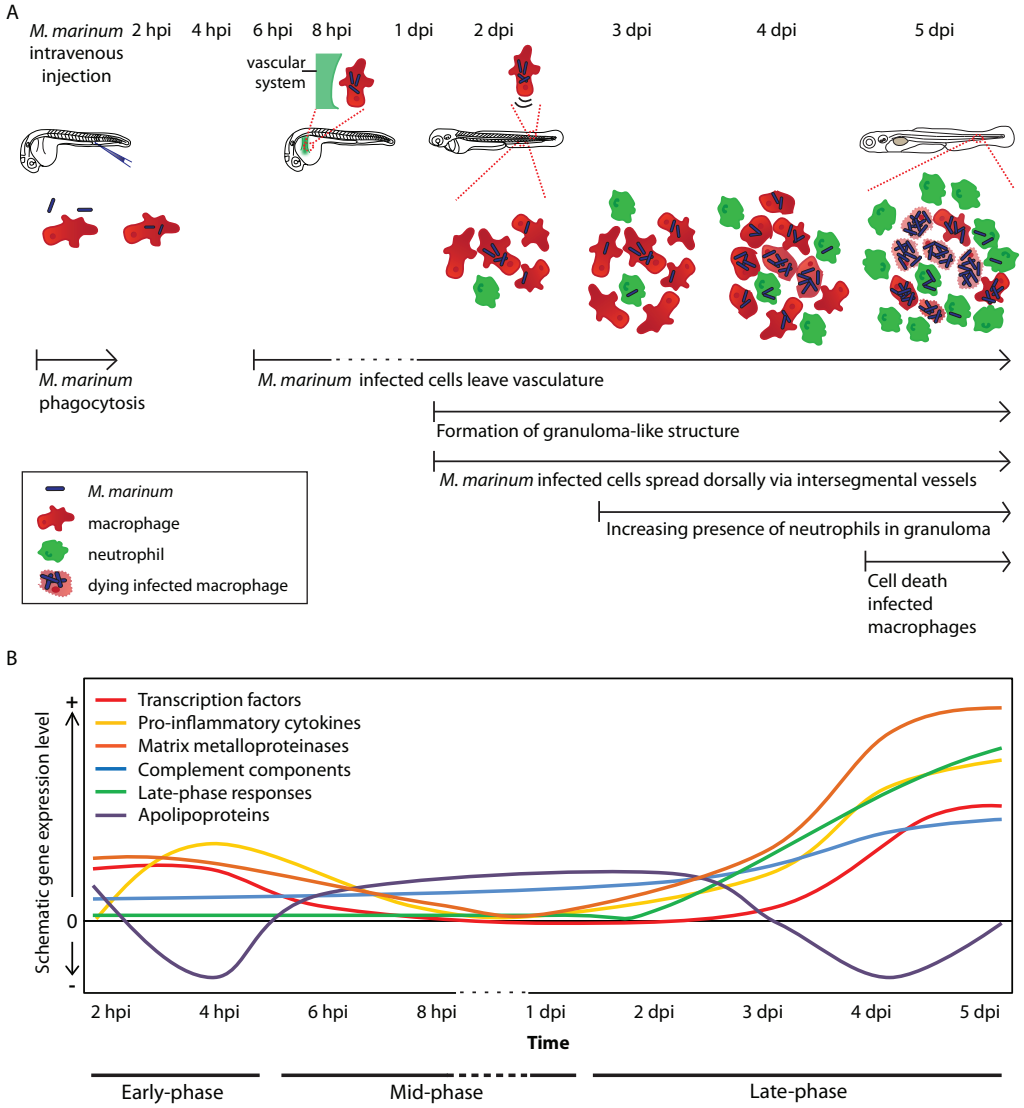

Figure 7. Infection process of *M. marinum*. A schematic overview representing (A) the observed host-pathogen interactions and (B) the gene expression profiles of transcription factors (red line), pro-inflammatory cytokines (yellow line), matrix metalloproteinases (orange line), complement components (blue line), late-phase responses (green line), and apolipoproteins (purple line).

GEO profiles in the NCBI database we find that *Atf3* expression is gradually induced in mice during early lung immune response to *M. tuberculosis* (GDS4257) and *ATF3* expression is induced in human macrophages in response to hypoxia (GDS2036). Hypoxia occurs in the environment of the human tuberculous granulomas and it may be responsible for *M. tuberculosis* dormancy in humans [79]. It was recently shown in mice that ROS-mediated super-induction of *ATF3* causes high susceptibility to bacterial infections through the suppression of interleukin 6 (IL-6) and that *ATF3*-/- mice are protected against bacterial infections [80]. Atf3 can also be induced by LPS in bone-marrow derived from mice and this induction was suggested to regulate TLR-stimulated inflammatory responses as part of a negative-feedback loop [2]. Similarly, we observe less *M. marinum* infection in *atf3* morphant zebrafish embryos (fig. 4), but we did not observe a strong effect of *atf3* knockdown on the transcriptional signature. However, we did observe a general down-regulation trend of a group of apolipoproteins (supplementary fig. 4) which is interesting because it was previously shown that apolipoprotein E for example can inhibit cell migration of smooth muscle cells [81]. In addition, we found that Atf3 functions in suppressing macrophage and neutrophil migration towards local damage-induced inflammation sites (fig. 5), a process that is also important in the *M. marinum*-granuloma environment. To determine whether such increased attraction of leukocytes to inflammatory sites also occurs during granuloma formation in the *atf3* morphants, we imaged this process in a double transgenic zebrafish line with fluorescent macrophages and neutrophils. Knockdown of *atf3* resulted in an attenuated infection level as soon as 2 dpi and leukocyte numbers seemed to be increased around the infection locations at 1 and 2 dpi. Although differences in granuloma structure are difficult to quantify due to high variation between individual granulomas within single embryos, these observations suggest that increased leukocyte recruitment during the early stage of infection might be responsible for better restriction of *M. marinum* growth in *atf3* morphants. In contrast, attenuated *M. marinum* infection under knockdown conditions of *mmp9* has been associated with impaired rather than enhanced macrophage recruitment [45]. This difference between the *atf3* and *mmp9* knockdown phenotypes might be explained by the timing of leukocyte recruitment. It is possible that enhanced early recruitment of neutrophils to the initiating granuloma in *atf3* morphants helps restricting *M. marinum* growth. In contrast, *mmp9*, which is induced by the mycobacterial secreted protein ESAT-6 [45], is probably more important at later stages, when macrophage recruitment promotes granuloma expansion. Further research is necessary to determine the precise function of Atf3 during *M. marinum* infection.

In summary, this study provides a detailed description of the observed host-pathogen interactions during *M. marinum* infection in zebrafish embryos and interrelates this with gene expression profiles obtained from RNA sequencing. We also demonstrate that Atf3, one of the transcription factors induced during the early- and late-phase of infection, antagonises the host control of *M. marinum* acute infections, indicating the strength of using gene expression profiles to identify key host genes involved in mycobacterial pathogenesis.

Acknowledgements

The authors would like to thank Georges Lutfalla (University Montpellier 2) for the kind gift of *Tg(mpeg1:mCherry-F)* fish, Ulrike Nehrdich, Laura van Hulst and Davy de Witt for fish care, and other lab members for helpful discussions. EB, HPS, and AHM were supported by the Smart Mix Program of the Netherlands Ministry of Economic Affairs and the Ministry of Education, Culture and Science, JR by a Marie Curie Fellowship of the European 7th Framework Initial Training Network FishForPharma (PITG-GA-2011-289209), and PIR by a Marie Curie Intra-European Fellowship (PIEF-GA-2010-274389).

References

1. Whitmore, M.M. *et al.* Negative regulation of TLR-signaling pathways by activating transcription factor-3. *Journal of immunology* **179**, 3622-3630 (2007).

2. Gilchrist, M. *et al.* Systems biology approaches identify ATF3 as a negative regulator of Toll-like receptor 4. *Nature* **441**, 173-178 (2006).

3. Ottenhoff, T.H. New pathways of protective and pathological host defense to mycobacteria. *Trends in microbiology* **20**, 419-428 (2012).

4. Cooper, A.M. & Torrado, E. Protection versus pathology in tuberculosis: recent insights. *Current opinion in immunology* **24**, 431-437 (2012).

5. Stinear, T.P. *et al.* Insights from the complete genome sequence of Mycobacterium marinum on the evolution of Mycobacterium tuberculosis. *Genome Res* **18**, 729-741 (2008).

6. Ruley, K.M. *et al.* Identification of Mycobacterium marinum virulence genes using signature-tagged mutagenesis and the goldfish model of mycobacterial pathogenesis. *FEMS microbiology letters* **232**, 75-81 (2004).

7. Tobin, D.M. & Ramakrishnan, L. Comparative pathogenesis of Mycobacterium marinum and Mycobacterium tuberculosis. *Cellular microbiology* **10**, 1027-1039 (2008).

8. Stamm, L.M. *et al.* Mycobacterium marinum escapes from phagosomes and is propelled by actin-based motility. *The Journal of experimental medicine* **198**, 1361-1368 (2003).

9. Leake, E.S., Myrvik, Q.N. & Wright, M.J. Phagosomal membranes of Mycobacterium bovis BCG-immune alveolar macrophages are resistant to disruption by Mycobacterium tuberculosis H37Rv. *Infection and immunity* **45**, 443-446 (1984).

10. Vergne, I., Chua, J., Singh, S.B. & Deretic, V. Cell biology of mycobacterium tuberculosis phagosome. *Annu Rev Cell Dev Biol* **20**, 367-394 (2004).

11. Simeone, R. *et al.* Phagosomal rupture by Mycobacterium tuberculosis results in toxicity and host cell death. *PLoS pathogens* **8**, e1002507 (2012).

12. van der Wel, N. *et al.* M. tuberculosis and M. leprae translocate from the phagolysosome to the cytosol in myeloid cells. *Cell* **129**, 1287-1298 (2007).

13. Ramakrishnan, L. Revisiting the role of the granuloma in tuberculosis. *Nat Rev Immunol* **12**, 352-366 (2012).

14. Parikka, M. *et al.* Mycobacterium marinum causes a latent infection that can be reactivated by gamma irradiation in adult zebrafish. *PLoS pathogens* **8**, e1002944 (2012).

15. Swaim, L.E. *et al.* Mycobacterium marinum Infection of Adult Zebrafish Causes Caseating Granulomatous Tuberculosis and Is Moderated by Adaptive Immunity. *Infection and Immunity* **74**, 6108-6117 (2006).

16. Davis, J.M. *et al.* Real-time visualization of mycobacterium-macrophage interactions leading to initiation of granuloma formation in zebrafish embryos. *Immunity* **17**, 693-702 (2002).

17. Berg, R.D. & Ramakrishnan, L. Insights into tuberculosis from the zebrafish model. *Trends Mol Med* **18**, 689-690 (2012).

18. Clay, H. *et al.* Dichotomous Role of the Macrophage in Early Mycobacterium marinum Infection of the Zebrafish. *Cell Host & Microbe* **2**, 29-39 (2007).

19. Volkman, H.E. *et al.* Tuberculous granuloma formation is enhanced by a mycobacterium virulence determinant. *PLoS Biol* **2**, e367 (2004).

20. Davis, J.M. & Ramakrishnan, L. The Role of the Granuloma in Expansion and Dissemination of Early Tuberculous Infection. *Cell* **136**, 37-49 (2009).

21. Traver, D. *et al.* The Zebrafish as a Model Organism to Study Development of the Immune System. **81**, 254-330 (2003).

22. Clay, H., Volkman, H.E. & Ramakrishnan, L. Tumor Necrosis Factor Signaling Mediates Resistance to Mycobacteria by Inhibiting Bacterial Growth and Macrophage Death. *Immunity* **29**, 283-294 (2008).

23. van der Vaart, M., van Soest, J.J., Spaink, H.P. & Meijer, A.H. Functional analysis of a zebrafish myd88 mutant identifies key transcriptional components of the innate immune system. *Dis Model Mech* **6**, 841-854 (2013).

24. Lawson, N.D. & Weinstein, B.M. In vivo imaging of embryonic vascular development using transgenic zebrafish. *Dev Biol* **248**, 307-318 (2002).

25. Renshaw, S.A. *et al.* A transgenic zebrafish model of neutrophilic inflammation. *Blood* **108**, 3976-3978 (2006).

26. Bernut, A. *et al.* Mycobacterium abscessus cording prevents phagocytosis and promotes abscess formation. *Proc Natl Acad Sci U S A* (2014).

27. d'Alençon, C.A. *et al.* A high-throughput chemically induced inflammation assay in zebrafish. *BMC Biology* **8**, 151 (2010).

28. van der Sar, A.M. *et al.* Mycobacterium marinum Strains Can Be Divided into Two Distinct Types Based on Genetic Diversity and Virulence. *Infection and Immunity* **72**, 6306-6312 (2004).

29. Kimmel, C.B., Ballard, W.W., Kimmel, S.R., Ullmann, B. & Schilling, T.F. Stages of embryonic development of the zebrafish. *Dev Dyn* **203**, 253-310 (1995).

30. Benard, E.L. *et al.* Infection of zebrafish embryos with intracellular bacterial pathogens. *J Vis Exp* **pii: 3781. doi: 10.3791/3781** (2012).

31. Veneman, W.J. *et al.* A zebrafish high throughput screening system used for Staphylococcus epidermidis infection marker discovery. *BMC Genomics* **14**, 255 (2013).

32. Stockhammer, O.W., Zakrzewska, A., Hegedus, Z., Spaink, H.P. & Meijer, A.H. Transcriptome profiling and functional analyses of the zebrafish embryonic innate immune response to Salmonella infection. *J Immunol* **182**, 5641-5653 (2009).

33. Zakrzewska, A. *et al.* Macrophage-specific gene functions in Spi1-directed innate immunity. *Blood* **116**, e1-11 (2010).

34. Ordas, A. *et al.* MicroRNA-146 function in the innate immune transcriptome response of zebrafish embryos to Salmonella typhimurium infection. *BMC genomics* **14**, 696 (2013).

35. Huang da, W., Sherman, B.T. & Lempicki, R.A. Systematic and integrative analysis of large gene lists using DAVID bioinformatics resources. *Nat Protoc* **4**, 44-57 (2009).

36. Kanwal, Z. *et al.* Deficiency in hematopoietic phosphatase ptpn6/Shp1 hyperactivates the innate immune system and impairs control of bacterial infections in zebrafish embryos. *J Immunol* **190**, 1631-1645 (2013).

37. Anders, S. & Huber, W. Differential expression analysis for sequence count data. *Genome biology* **11**, R106 (2010).

38. Mariathasan, S. & Monack, D.M. Inflammasome adaptors and sensors: intracellular regulators of infection and inflammation. *Nat Rev Immunol* **7**, 31-40 (2007).

39. Mayer-Barber, K.D. *et al.* Caspase-1 independent IL-1beta production is critical for host resistance to mycobacterium tuberculosis and does not require TLR signaling in vivo. *Journal of immunology* **184**, 3326-3330 (2010).

40. Kinoshita, S., Biswas, G., Kono, T., Hikima, J. & Sakai, M. Presence of two tumor necrosis factor (tnf)-alpha homologs on different chromosomes of zebrafish (Danio rerio) and medaka (Oryzias latipes). *Mar Genomics* **13**, 1-9 (2014).

41. Tobin, D.M. *et al.* The lta4h Locus Modulates Susceptibility to Mycobacterial Infection in Zebrafish and Humans. *Cell* **140**, 717-730 (2010).

42. Deng, Q. *et al.* Localized bacterial infection induces systemic activation of neutrophils through Cxcr2 signaling in zebrafish. *Journal of leukocyte biology* **93**, 761-769 (2013).

43. de Oliveira, S. *et al.* Cxcl8 (IL-8) mediates neutrophil recruitment and behavior in the zebrafish inflammatory response. *Journal of immunology* **190**, 4349-4359 (2013).

44. Elkington, P.T., O'Kane, C.M. & Friedland, J.S. The paradox of matrix metalloproteinases in infectious disease. *Clin Exp Immunol* **142**, 12-20 (2005).

45. Volkman, H.E. *et al.* Tuberculous granuloma induction via interaction of a bacterial secreted protein with host epithelium. *Science* **327**, 466-469 (2010).

46. Brew, K., Dinakarpandian, D. & Nagase, H. Tissue inhibitors of metalloproteinases: evolution, structure and function. *Biochim Biophys Acta* **1477**, 267-283 (2000).

47. Wang, Z., Zhang, S., Tong, Z., Li, L. & Wang, G. Maternal transfer and protective role of the alternative complement components in zebrafish Danio rerio. *PloS one* **4**, e4498 (2009).

48. Hall, C.J. *et al.* Immunoresponsive gene 1 augments bactericidal activity of macrophage-lineage cells by regulating beta-oxidation-dependent mitochondrial ROS production. *Cell Metab* **18**, 265-278 (2013).

49. Urieli-Shoval, S., Linke, R.P. & Matzner, Y. Expression and function of serum amyloid A, a major acute-phase protein, in normal and disease states. *Curr Opin Hematol* **7**, 64-69 (2000).

50. Hegedus, Z. *et al.* Deep sequencing of the zebrafish transcriptome response to mycobacterium infection. *Molecular immunology* **46**, 2918-2930 (2009).

51. Stockhammer, O.W. *et al.* Transcriptome analysis of Traf6 function in the innate immune response of zebrafish embryos. *Mol Immunol* **48**, 179-190 (2010).

52. Wellen, K.E. *et al.* Coordinated regulation of nutrient and inflammatory responses by STAMP2 is essential for metabolic homeostasis. *Cell* **129**, 537-548 (2007).

53. Zhang, J., Yu, L.P., Li, M.F. & Sun, L. Turbot (Scophthalmus maximus) hepcidin-1 and hepcidin-2 possess antimicrobial activity and promote resistance against bacterial and viral infection. *Fish & shellfish immunology* (2014).

54. van der Vaart, M. *et al.* The DNA Damage-Regulated Autophagy Modulator DRAM1 Links Mycobacterial Recognition via TLP-MYD88 to Authophagic Defense. *Cell host & microbe* **15**, 753-767 (2014).

55. Zhang, C. *et al.* Transcriptional activation of the human stress-inducible transcriptional repressor ATF3 gene promoter by p53. *Biochemical and biophysical research communications* **297**, 1302-1310 (2002).

56. van der Vaart, M., Spaink, H.P. & Meijer, A.H. Pathogen recognition and activation of the innate immune response in zebrafish. *Adv Hematol* **2012**, 159807 (2012).

57. Schlesinger, L.S. Macrophage phagocytosis of virulent but not attenuated strains of Mycobacterium tuberculosis is mediated by mannose receptors in addition to complement receptors. *J Immunol* **150**, 2920-2930 (1993).

58. Schlesinger, L.S., Bellinger-Kawahara, C.G., Payne, N.R. & Horwitz, M.A. Phagocytosis of Mycobacterium tuberculosis is mediated by human monocyte complement receptors and complement component C3. *J Immunol* **144**, 2771-2780 (1990).

59. Maeda, N. *et al.* The cell surface receptor DC-SIGN discriminates between Mycobacterium species through selective recognition of the mannose caps on lipoarabinomannan. *The Journal of biological chemistry* **278**, 5513-5516 (2003).

60. Schonbeck, U., Mach, F. & Libby, P. Generation of biologically active IL-1 beta by matrix metalloproteinases: a novel caspase-1-independent pathway of IL-1 beta processing. *Journal of immunology* **161**, 3340-3346 (1998).

61. Ito, A. *et al.* Degradation of interleukin 1beta by matrix metalloproteinases. *The Journal of biological chemistry* **271**, 14657-14660 (1996).

62. Sternlicht, M.D. & Werb, Z. How matrix metalloproteinases regulate cell behavior. *Annu Rev Cell Dev Biol* **17**, 463-516 (2001).

63. Chang, J.C. *et al.* Effect of Mycobacterium tuberculosis and its components on macrophages and the release of matrix metalloproteinases. *Thorax* **51**, 306-311 (1996).

64. Rivera-Marrero, C.A., Schuyler, W., Roser, S. & Roman, J. Induction of MMP-9 mediated gelatinolytic activity in human monocytic cells by cell wall components of Mycobacterium tuberculosis. *Microbial pathogenesis* **29**, 231-244 (2000).

65. Quiding-Jarbrink, M., Smith, D.A. & Bancroft, G.J. Production of matrix metalloproteinases in response to mycobacterial infection. *Infection and immunity* **69**, 5661-5670 (2001).

66. Hrabec, E., Strek, M., Zieba, M., Kwiatkowska, S. & Hrabec, Z. Circulation level of matrix metalloproteinase-9 is correlated with disease severity in tuberculosis patients. *Int J Tuberc Lung Dis* **6**, 713-719 (2002).

67. Price, N.M. *et al.* Identification of a matrix-degrading phenotype in human tuberculosis in vitro and in vivo. *Journal of immunology* **166**, 4223-4230 (2001).

68. Price, N.M., Gilman, R.H., Uddin, J., Recavarren, S. & Friedland, J.S. Unopposed matrix metalloproteinase-9 expression in human tuberculous granuloma and the role of TNF-alpha-dependent monocyte networks. *Journal of immunology* **171**, 5579-5586 (2003).

69. Izzo, A.A., Izzo, L.S., Kasimos, J. & Majka, S. A matrix metalloproteinase inhibitor promotes granuloma formation during the early phase of Mycobacterium tuberculosis pulmonary infection. *Tuberculosis (Edinb)* **84**, 387-396 (2004).

70. Tobin, D.M. *et al.* Host genotype-specific therapies can optimize the inflammatory response to mycobacterial infections. *Cell* **148**, 434-446 (2012).

71. Beatty, W.L., Ullrich, H.J. & Russell, D.G. Mycobacterial surface moieties are released from infected macrophages by a constitutive exocytic event. *Eur J Cell Biol* **80**, 31-40 (2001).

72. van den Elzen, P. *et al.* Apolipoprotein-mediated pathways of lipid antigen presentation. *Nature* **437**, 906-910 (2005).

73. Geisel, R.E., Sakamoto, K., Russell, D.G. & Rhoades, E.R. In vivo activity of released cell wall lipids of Mycobacterium bovis bacillus Calmette-Guerin is due principally to trehalose mycolates. *Journal of immunology* **174**, 5007-5015 (2005).

74. Zhang, S. & Cui, P. Complement system in zebrafish. *Developmental and comparative immunology* (2014).

75. Elks, P.M. *et al.* Hypoxia inducible factor signaling modulates susceptibility to mycobacterial infection via a nitric oxide dependent mechanism. *PLoS pathogens* **9**, e1003789 (2013).

76. Yang, C.T. *et al.* Neutrophils exert protection in the early tuberculous granuloma by oxidative killing of mycobacteria phagocytosed from infected macrophages. *Cell Host Microbe* **12**, 301-312 (2012).

77. Chen, B.P., Liang, G., Whelan, J. & Hai, T. ATF3 and ATF3 delta Zip. Transcriptional repression versus activation by alternatively spliced isoforms. *The Journal of biological chemistry* **269**, 15819-15826 (1994).

78. Seimon, T.A. *et al.* Induction of ER stress in macrophages of tuberculosis granulomas. *PloS one* **5**, e12772 (2010).

79. Boshoff, H.I. & Barry, C.E., 3rd Tuberculosis - metabolism and respiration in the absence of growth. *Nat Rev Microbiol* **3**, 70-80 (2005).

80. Hoetzenecker, W. *et al.* ROS-induced ATF3 causes susceptibility to secondary infections during sepsis-associated immunosuppression. *Nat Med* **18**, 128-134 (2012).

81. Hui, D.Y. & Basford, J.E. Distinct signaling mechanisms for apoE inhibition of cell migration and proliferation. *Neurobiol Aging* **26**, 317-323 (2005).

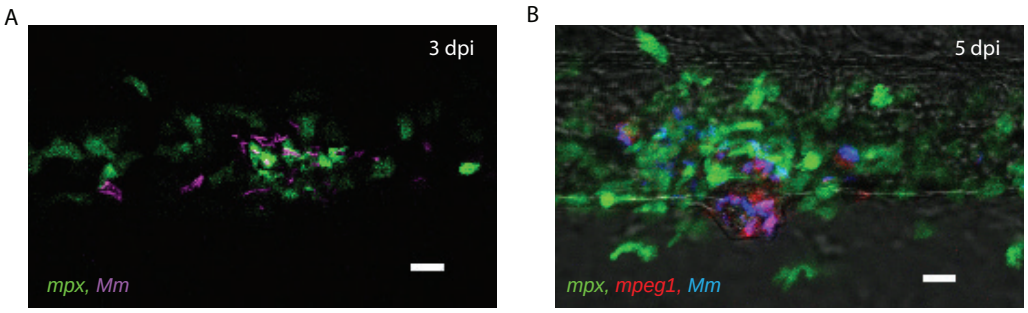

Supplementary figure 1. Granuloma contains infected neutrophils at 3 dpi and grows outside the vasculature at 5 dpi. (A) Neutrophils (*Tg(mpx:GFP)*) containing *M. marinum* (mCherry-expressing Mma20 depicted in magenta) at 3 dpi in granuloma of infected embryo from figure 1R. Z-stack maximum intensity projection of slices 9-18 of 27 total. (B) Granuloma from E2-Crimson-expressing *M. marinum* M-strain (depicted in blue) infected *Tg(mpx:GFP)/Tg(mpeg1:mCherry-F)* embryo at 5 dpi from figure 1T. Bacterial infection can be seen in cluster extending outwards from the tail region of the embryo. Scale bars: 20 µm.

Supplementary figure 2. Overview of expression profiles during *M. marinum* infection of gene groups additional to those shown in Fig. 3. Gene expression levels of groups of selected genes during a time course of *M. marinum* infection are represented as log2 fold change values. Groups of genes represented are: (A) ADAM metalloproteinases; (B) acute phase response, other than complement; (C) prostaglandin biosynthetic genes and receptors (late response); (D) negative regulators (late response); (E) NADPH oxidase complex genes. Statistically significant data points (adjusted P-value <0.1) are indicated below the x-axis as the shape filled with the colour of the specific gene (see legend for gene shape and colour). Only genes are shown for which differential expression was significant in at least one time point (F-I) qPCR validation of expression levels of (F) *il1b*, (G) *il8*, (H) *mmp9*, and (I) *apoa4*.

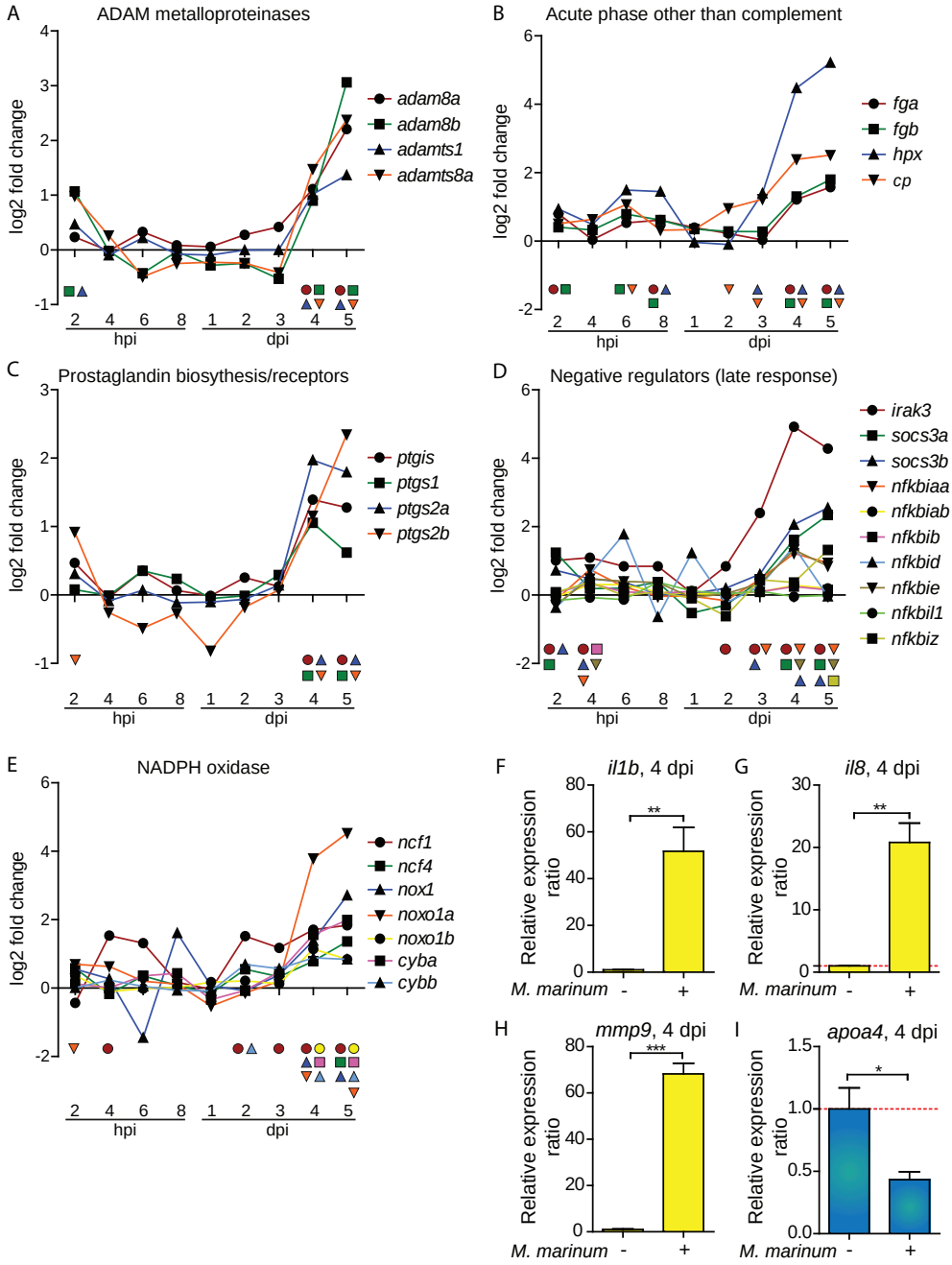
A
ADAM metalloproteinases
log2 fold change
adam8a
adam8b
adamts1
adamts8a
hpi
dpi
B
Acute phase other than complement
fga
fgb
hpx
cp
C
Prostaglandin biosythesis/receptors
ptgis
ptgs1
ptgs2a
ptgs2b
D
Negative regulators (late response)
irak3
socs3a
socs3b
nfkbiaa
nfkbiab
nfkbib
nfkbid
nfkbie
nfkbil1
nfkbiz
E
NADPH oxidase
ncf1
ncf4
nox1
noxo1a
noxo1b
cyba
cybb
F
il1b, 4 dpi
Relative expression ratio
M. marinum
G
il8, 4 dpi
H
mmp9, 4 dpi
I
apoa4, 4 dpi

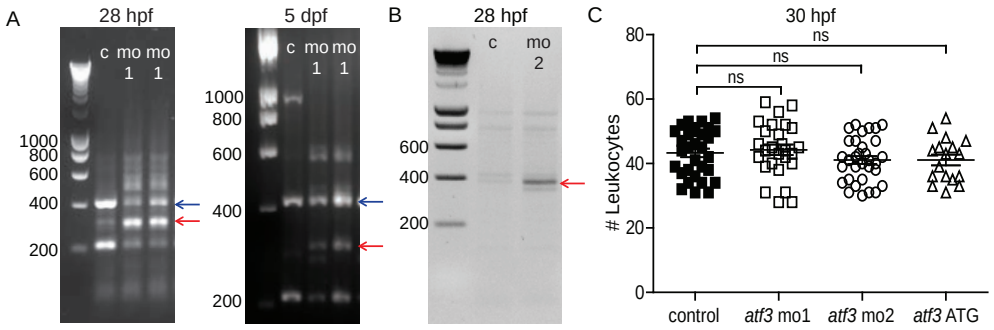

Supplementary figure 3. Validation of *atf3* morpholino knockdown. (A-B) Knockdown of *atf3*. Expression of *atf3* was determined by RT-PCR using RNA from embryos injected with (A) *atf3* morpholino 1 (Mo1) or control morpholino (c) at 28 hpf and 5 dpf or with (B) *atf3* morpholino 2 (Mo2) or control morpholino (c) at 28 hpf. (A) Blue arrow indicates control RT-PCR product size (425 bp) and red arrow indicates morpholino 1 knockdown predicted product size (317 bp). (B) Red arrow indicates RT-PCR product designed to amplify included intron during atf3 morpholino 2 knockdown (374 bp) on the right. (C) Normal leukocyte numbers in *atf3* morphants. *atf3* morphants and control embryos were fixed at 30 hpf and were immuno-labelled with Ab against the general leukocyte marker L-plastin. Leukocyte numbers were counted blinded in the tail (ns = not significant).

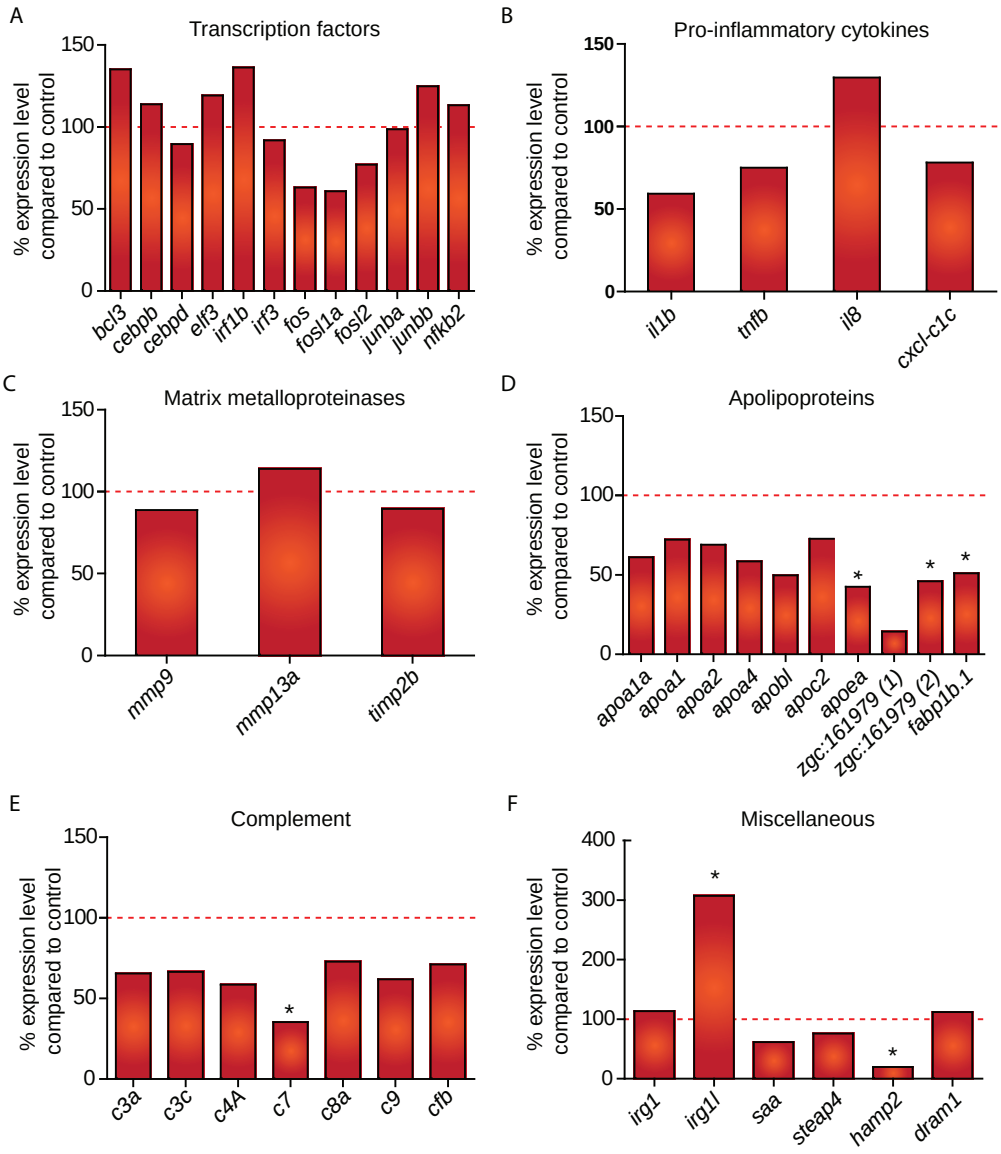

Supplementary figure 4. Effect of *atf3* knockdown on immune response at 4 dpi. The expression level of selected genes (identical to those in fig. 3) under conditions of *atf3* deficiency is expressed as the percentage of the expression level in the corresponding control. Results are based on RNA-Seq analysis of pools of 30 infected and 30 uninfected embryos for each group. Embryos were injected with *M. marinum* Mma20 (250 cfu) or mock injected with 2% PVP, and RNA-Seq analysis was performed at 4 dpi. Asterisks indicate significant difference.

Supplementary table 1: Gene ontology and KEGG pathways enriched in infected embryos

Gene ID	Gene name	Description
Matrix metalloproteinases and inhibitors		
ENSDARG00000042816	*mmp9*	matrix metalloproteinase 9
ENSDARG00000012395	*mmp13a*	matrix metalloproteinase 13a
ENSDARG00000075261	*timp2b*	tissue inhibitor of metalloproteinase 2b
Cytokines		
ENSDARG00000005419	*il1b*	interleukin 1, beta
ENSDARG00000009511	*tnfa*	tumor necrosis factor a (TNF superfamily, member 2)
ENSDARG00000013598	*tnfb*	tumor necrosis factor b (TNF superfamily, member 2)
ENSDARG00000100007	*il8*	interleukin 8
CXCL chemokines		
ENSDARG00000075045	*cxcl-c1c*	chemokine (C-X-C motif) ligand C1c
Transcription factors		
ENSDARG00000007823	*atf3*	activating transcription factor 3
ENSDARG00000087832	*bcl3*	B-cell CLL/lymphoma 3
ENSDARG00000042725	*cebpb*	CCAAT/enhancer binding protein (C/EBP), beta
ENSDARG00000087303	*cebpd*	CCAAT/enhancer binding protein (C/EBP), delta
ENSDARG00000077982	*elf3*	E74-like factor 3 (ets domain transcription factor, epithelial-specific)
ENSDARG00000032768	*irf1b*	interferon regulatory factor 1b
ENSDARG00000076251	*irf3*	interferon regulatory factor 3
ENSDARG00000031683	*fos*	v-fos FBJ murine osteosarcoma viral oncogene homolog
ENSDARG00000015355	*fosl1*	FOS-like antigen 1
ENSDARG00000040623	*fosl2*	fos-like antigen 2
ENSDARG00000074378	*junba*	jun B proto-oncogene a
ENSDARG00000088371	*junbb*	jun B proto-oncogene b
ENSDARG00000038687	*nfkb2*	nuclear factor of kappa light polypeptide gene enhancer in B-cells 2, p49/p100
Lipid transport		
ENSDARG00000012076	*apoa1a*	apolipoprotein A-Ia
ENSDARG00000086583	*apoa1 (2 of 2)*	apolipoprotein A-I
ENSDARG00000015866	*apoa2*	apolipoprotein A-II
ENSDARG00000040298	*apoa4*	apolipoprotein A-IV
ENSDARG00000022767	*apobl/apobb*	apolipoprotein B, like
ENSDARG00000092155	*apoc2*	apolipoprotein C-II
ENSDARG00000086370	*apoea*	apolipoprotein Ea
ENSDARG00000041490	*zgc:161979 (1)*	apolipoprotein A-II family
ENSDARG00000095863	*zgc:161979 (2)*	apolipoprotein A-II family
ENSDARG00000059227	*fabp1b.1*	fatty acid binding protein 1b, tandem duplicate 1
Complement		
ENSDARG00000012694	*c3a*	complement component c3a
ENSDARG00000052207	*c3c*	complement component c3c
ENSDARG00000038424	*c4a*	complement component 4A (Rodgers blood group)
ENSDARG00000057121	*c7 (2 of 2)*	complement component 7
ENSDARG00000039516	*c8a*	complement component 8, alpha polypeptide
ENSDARG00000016319	*c9*	complement component 9
ENSDARG00000055278	*cfb*	complement factor B
irg1 and irg1l		
ENSDARG00000069844	*irg1*	immunoresponsive gene 1
ENSDARG00000062788	*irg1l*	immunoresponsive gene 1, like
Miscellaneous		
ENSDARG00000045999	*saa*	serum amyloid A
ENSDARG00000055901	*steap4*	STEAP family member 4
ENSDARG00000053227	*hamp2*	hepcidin antimicrobial peptide 2
Autophagy		
ENSDARG00000045561	*dram1*	DNA-damage regulated autophagy modulator 1

ADAM metalloproteinases		
ENSDARG00000001452	*adam8a*	a disintegrin and metalloproteinase domain 8a
ENSDARG00000057644	*adam8b*	a disintegrin and metalloproteinase domain 8b
ENSDARG00000041566	*adamts1*	ADAM metallopeptidase with thrombospondin type 1 motif, 1
ENSDARG00000007709	*adamts8a*	ADAM metallopeptidase with thrombospondin type 1 motif, 8a
Acute phase other than complement		
ENSDARG00000020741	*fga*	fibrinogen alpha chain
ENSDARG00000008969	*fgb*	fibrinogen, B beta polypeptide
ENSDARG00000051912	*hpx (1 of 2)*	hemopexin
ENSDARG00000010312	*cp*	ceruloplasmin
prostaglandin biosythesis/receptors		
ENSDARG00000060094	*ptgis*	prostaglandin I2 (prostacyclin) synthase
ENSDARG00000052148	*ptgs1*	prostaglandin-endoperoxide synthase 1
ENSDARG00000004539	*ptgs2a*	prostaglandin-endoperoxide synthase 2a
ENSDARG00000010276	*ptgs2b*	prostaglandin-endoperoxide synthase 2b
negative regulators (late response)		
ENSDARG00000053131	*irak3*	interleukin-1 receptor-associated kinase 3
ENSDARG00000025428	*socs3a*	suppressor of cytokine signaling 3a
ENSDARG00000026611	*socs3b*	suppressor of cytokine signaling 3b
ENSDARG00000005481	*nfkbiaa*	nuclear factor of kappa light polypeptide gene enhancer in B-cells inhibitor, alpha a
ENSDARG00000007693	*nfkbiab*	nuclear factor of kappa light polypeptide gene enhancer in B-cells inhibitor, alpha b
ENSDARG00000030087	*nfkbib*	nuclear factor of kappa light polypeptide gene enhancer in B-cells inhibitor, beta
ENSDARG00000077001	*nfkbid*	nuclear factor of kappa light polypeptide gene enhancer in B-cells inhibitor, delta
ENSDARG00000068367	*nfkbie*	nuclear factor of kappa light polypeptide gene enhancer in B-cells inhibitor, epsilon
ENSDARG00000003157	*nfkbil1*	nuclear factor of kappa light polypeptide gene enhancer in B-cells inhibitor-like 1
ENSDARG00000095117	*nfkbiz*	nuclear factor of kappa light polypeptide gene enhancer in B-cells inhibitor, zeta
NADPH oxidase		
ENSDARG00000033735	*ncf1*	neutrophil cytosolic factor 1 (p47phox)
ENSDARG00000040812	*ncf4*	neutrophil cytosolic factor 4 (p40phox)
ENSDARG00000070062	*nox1*	NADPH oxidase 1
ENSDARG00000041294	*noxo1a*	NADPH oxidase organizer 1a
ENSDARG00000056374	*noxo1b*	NADPH oxidase organizer 1b
ENSDARG00000018283	*cyba*	cytochrome b-245, alpha polypeptide (p22phox)
ENSDARG00000056615	*cybb*	cytochrome b-245, beta polypeptide (p91phox, chronic granulomatous disease)

Footnote: table of gene IDs, names and descriptions of selected genes that are presented in this research (fig. 3 and supplementary fig. 2). * *zgc:161979* (1) and (2) are two paralogues of an apolipoprotein A-II family gene on chromosome 16.

Supplementary movie S1. E2-Crimson-expressing *M. marinum* bacterial infection in *Tg(fli1a:EGFP)/Tg(mpeg1:mCherry-F)*. A z-stack was imaged every 20 minutes at the caudal vein from 180 minutes post infection (mpi) to 820 mpi and is presented as a maximum intensity z-stack projection of the merged E2-Crimson, EGFP and mCherry channels. At 400 minutes an infected macrophage (purple: overlapping E2-Crimson and mCherry) can be seen outside the vasculature. Supplementary movie can be viewed at: https://www.dropbox.com/sh/1zwu4b6f1uzeuap/Ftc9uFKwpG?n=26155020